

# MEASURING THE GALAXY POWER SPECTRUM WITH FUTURE REDSHIFT SURVEYS

MAX TEGMARK<sup>a</sup>

<sup>a</sup>Hubble Fellow.

Institute for Advanced Study, Princeton, NJ 08540; max@ias.edu

ANDREW J. S. HAMILTON

JILA and Dept. of Astrophysical, Planetary and Atmospheric Sciences,  
 Box 440, Univ. of Colorado, Boulder, CO 80309, USA; ajsh@dark.colorado.edu  
 MICHAEL A. STRAUSS<sup>a</sup>

<sup>a</sup>Alfred P. Sloan Foundation Fellow.

Department of Astrophysical Sciences, Princeton University, Princeton, NJ 08544;  
 strauss@astro.princeton.edu

MICHAEL S. VOGLEY<sup>1</sup>

Department of Astrophysical Sciences, Princeton University, Princeton, NJ 08544;  
 vogeley@astro.princeton.edu

AND

ALEXANDER S. SZALAY

Department of Physics and Astronomy, Johns Hopkins University, Baltimore, MD 21218; szalay@pha.jhu.edu

*August 3, 1997. Submitted to ApJ.*

## ABSTRACT

Precision measurements of the galaxy power spectrum  $P(k)$  require a data analysis pipeline that is both fast enough to be computationally feasible and accurate enough to take full advantage of high-quality data. We present a rigorous discussion of different methods of power spectrum estimation, with emphasis on traditional, Karhunen-Loève, and quadratic schemes, showing in what approximations they give the same result. To improve speed, we show how many of the advantages of Karhunen-Loève power spectrum estimation may be achieved with a computationally faster quadratic method. To improve accuracy, we derive analytic expressions for handling the integral constraint, since it is crucial that finite volume effects are accurately corrected for on scales comparable to the depth of the survey. We also show that for the Karhunen-Loève and quadratic techniques, multiple constraints can be included via simple matrix operations, thereby rendering the results less sensitive to galactic extinction and misestimates of the radial selection function. We present a data analysis pipeline that we argue does justice to the increases in both quality and quantity of data that upcoming redshift surveys will provide. It involves using three analysis techniques in conjunction: a traditional Fourier approach on small scales, a pixelized quadratic matrix method on large scales and a pixelized Karhunen-Loève eigenmode analysis to probe anisotropic effects such as redshift-space distortions.

## 1. INTRODUCTION

Observational data on galaxy clustering are rapidly increasing in both quantity and quality, which brings new challenges to data analysis. As for quantity, redshifts had been published for a few thousand galaxies 15 years ago. Today the number is  $\sim 10^5$  (Huchra, private communication), and ongoing projects such as the AAT 2dF Survey and the Sloan Digital Sky Survey (hereafter SDSS; see Gunn & Weinberg 1995) will raise it to  $10^6$  in a few years. Comprehensive reviews of past redshift surveys are given by Efsthathiou (1994), Vogeley (1995), Strauss & Willick (1995) and Strauss (1997), the last also including a detailed description of 2dF and SDSS. As for quality, more accurate and uniform photometric selection criteria (enabled by *e.g.* the well-calibrated 5-band photometry of the SDSS) reduce potential systematic errors. This increased data quality makes it desirable to avoid approximations in the data analysis process and to use methods that can constrain cosmological quantities as accurately as possible. This is especially important since a wide variety of mod-

els currently appear to be at least marginally consistent with the present data (Peacock 1997; White *et al.* 1996; Vogeley 1997), so smaller error bars on the power spectrum will be needed to discriminate between them. However, the increased data quantity makes it a real challenge to perform such an accurate analysis; as we will discuss at some length, a straightforward application of any such method is computationally unfeasible for data sets as large as those from 2dF and SDSS.

This paper addresses both the accuracy and speed issues for measuring the galaxy power spectrum  $P(k)$ . For the highest accuracy, we advocate the use of lossless pixelized methods, both linear (Karhunen-Loève) and quadratic. To improve the speed, we present a fast implementation of a pixelized quadratic power estimation method, and show how it can reproduce Karhunen-Loève results (Vogeley & Szalay 1996; Tegmark, Taylor & Heavens 1997 — hereafter TTH) exactly, without the need to solve eigenvalue problems, although it does not have the ability to measure redshift-space distortions.

The rest of the paper is organized as follows. Section 2 is a “buyers guide”, where we list the various properties that are important when deciding which data analysis method to use. In Section 3, we review the existing methods for power spectrum estimation in a common framework, make various extensions of them and present the fast quadratic power spectrum technique. Section 4 describes how the various methods are interrelated, and Section 5 discusses how they can be immunized from various systematic effects, such as errors in the extinction model; many of the technical details are given in Appendices A and B. Section 6 discusses the pros and cons of the different techniques. We conclude that to meet all criteria on the wish list of Section 2, it is necessary to combine three of the principal methods described. The data analysis pipeline that we propose is summarized in Figure D1, and the reader may wish to glance at this before delving into the details of Section 3, to obtain an overview of how everything fits together.

## 2. COMPARING METHODS: A WISH LIST

Since the ultimate goal of the analysis of clustering in a galaxy redshift survey is to constrain cosmological models, we want a method that minimizes the statistical error bars on cosmological parameters<sup>1</sup> and is robust against potential systematic errors. We will now discuss the former issue in some detail, and return to the latter in Section 5 and Appendix B.

### 2.1. The traditional approach

Let us parametrize the power spectrum  $P(k)$  by some set of parameters  $\theta_i, i = 1, 2, \dots$ , grouped into a vector  $\Theta$ . These may be either the band powers in a set of narrow bands, or physically motivated parameters such as the normalization  $\sigma_8$ , the shape parameter  $\Gamma$ , the primordial spectral index  $n$ , *etc.* Let us package our data set into a vector  $\mathbf{x}$ ; much of the distinction between different methods discussed in Section 3 lies in the way this packaging is done. The standard approach to parameter estimation is to write down the expression for the probability distribution  $f(\mathbf{x}; \Theta)$ . Here we interpret  $f$  as a probability distribution over  $\mathbf{x}$  for a fixed  $\Theta$ . In a Bayesian statistical analysis with a uniform prior probability distribution for  $\Theta$ , one reinterprets  $f$  as a probability distribution over  $\Theta$  for a given data set  $\mathbf{x}$ , and to clarify this distinction renames  $f$  the likelihood function. The final results are often presented as contour plots of this likelihood function, as at the bottom of Figure 1.

If we take  $\mathbf{x}$  to be the raw data set, *i.e.*, the measured coordinates  $\mathbf{r}_\alpha$  ( $\alpha = 1, \dots, N$ ) in redshift space of the  $N$  measured galaxies, then the likelihood function  $f$  is unfortunately hopeless to compute numerically, since it involves the  $N$ -point correlation function. Even in the Gaussian approximation that  $f$  is given by a product over two-point correlation functions (e.g., Fry 1984), this requires evaluating a multivariate polynomial of degree  $N/2$  in the correlations of the  $N(N+1)/2$  galaxy pairs. The traditional approach has therefore been to take  $\mathbf{x}$  to be something else: band-power estimates of the power spectrum. These

are essentially computed by multiplying the observed density field by some weight function, Fourier transforming it, taking the squared modulus of the result and averaging over shells in  $k$ -space (Section 3.3). In the (sometimes poor) approximation that the probability distribution for  $\mathbf{x}$  is a multivariate Gaussian, its probability distribution is

$$f(\mathbf{x}; \Theta) \propto |\mathbf{C}|^{-1/2} e^{-\frac{1}{2}(\mathbf{x}-\mathbf{m})^t \mathbf{C}^{-1}(\mathbf{x}-\mathbf{m})}, \quad (1)$$

where  $|\mathbf{C}|$  denotes the determinant of  $\mathbf{C}$ , and the mean vector  $\mathbf{m} \equiv \langle \mathbf{x} \rangle$  and the covariance matrix  $\mathbf{C} \equiv \langle \mathbf{x}\mathbf{x}^t \rangle - \mathbf{m}\mathbf{m}^t$  depend on  $P(k)$  and hence on the unknown parameters  $\Theta$ . Much of the model testing to date has been rather approximate, often little more than a “chi-by-eye” fit of theoretical power spectra to the data, which is tantamount to ignoring the correlations between the power estimates (the off-diagonal elements of  $\mathbf{C}$ ). This approach clearly does not utilize all the information present in the data, and can also bias the results.

If we had infinite computer resources, we would improve the situation by simply performing an exact brute force likelihood analysis on the raw data set. Is there a faster way of obtaining the same result?

### 2.2. The notion of a lossless method

We will call a method for analyzing a data set *unbeatable* or *optimal* if no other method can place tighter constraints on cosmological models using this data.

#### 2.2.1. The Fisher Information Matrix

This can be made precise using the formalism of the *Fisher information matrix* (see TTH for a comprehensive review of this application), which offers a simple and a useful way of measuring how much information each step in the pipeline of Figure 1 destroys. Given any set of cosmological parameters of interest denoted  $\theta_i, i = 1, 2, \dots$ , their Fisher matrix  $\mathbf{F}$  gives the smallest error bars with which the parameters can possibly be measured from a given data set. If the probability distribution for the data set given the parameter values is  $f(\mathbf{x}; \Theta)$ , then the Fisher matrix is defined by (Fisher 1935)

$$\mathbf{F}_{ij} \equiv - \left\langle \frac{\partial^2 \ln f}{\partial \theta_i \partial \theta_j} \right\rangle. \quad (2)$$

Crudely speaking,  $\mathbf{F}^{-1}$  can be thought of as the best possible covariance matrix for the measurement errors on the parameters. Indeed, the Cramér-Rao inequality (Kenney & Keeping 1951; Kendall & Stuart 1969) states that no unbiased method whatsoever can measure the  $i^{\text{th}}$  parameter with error bars (standard deviation) less than  $1/\sqrt{\mathbf{F}_{ii}}$ . If the other parameters are not known but are estimated from the data as well, the minimum standard deviation rises to  $(\mathbf{F}^{-1})_{ii}^{1/2}$ . This formalism has recently been used to assess the accuracy with which cosmological parameters can be measured from future galaxy surveys (Tegmark 1997b; Goldberg & Strauss 1997) and cosmic microwave background experiments (Jungman *et al.* 1996; Bond, Efstathiou, & Tegmark 1997; Zaldarriaga, Seljak, & Spergel 1997).

<sup>1</sup>This is not a mere unimportant detail, since doubling the error bars (which an inferior method can easily do) is comparable to reducing the survey volume and the number of galaxies probed by a factor of four.

### 2.2.2. Checking for leaks in the pipeline

By computing the Fisher matrix separately from each of the intermediate data sets in Figure 1, we can track the flow of information down the data pipeline and check for leaks. For instance, if the Fisher matrix computed from the raw redshift data is identical to that computed from the (much smaller) data set consisting of the band power estimates, then the power spectrum estimation method is *lossless* in the sense that no information about the parameters of interest has been lost in the process of compressing the data set from, say,  $10^6$  numbers down to 50; cf., the discussion in Section 2.3. We will frequently use this criterion when comparing different data analysis techniques below.

### 2.2.3. The power spectrum Fisher matrix

Whether a method is lossless or not generally depends on which parameters we are interested in estimating. Fortunately, as shown by Tegmark (1997a, hereafter T97), certain methods can be shown to be lossless for *any* set of parameters in a large class. An important special case are quantities that parametrize the power spectrum  $P(k)$ , such as  $\sigma_8$  and  $\Gamma$ ; all the information on these parameters is retained if the power spectrum itself (parametrized by the power in many narrow bands) can be measured with the minimal error bars. This means that one can test whether a method is lossless simply by computing the Fisher matrix for the band powers. This also means that band powers have a special status compared to other parameters: if we simply measure  $P(k)$  as accurately as possible, this measured function will retain all the information about all cosmological parameters. However, these methods *do* lose information about parameters that affect the data set not only via  $P(k)$ . Important examples to which we will return are redshift-space distortions and uncorrected galactic extinction, both of which introduce differences between the angular and radial clustering patterns.

### 2.3. Data compression, simplicity and speed

A second and rather obvious criterion for comparing data analysis methods is their numerical feasibility. For instance, the brute-force likelihood analysis of the raw data set (the galaxy positions) described above is essentially lossless, but too time-consuming to be numerically feasible when  $N$ , the number of galaxies, is large.

When the brute-force method is unfeasible, the general approach is to perform some form of *data compression*, whereby the data set is reduced to a smaller and simpler one which is easier to analyze. If the data compression step is lossless, a brute-force analysis on the compressed data set clearly gives just as small error bars as one on the raw data would have done.

To facilitate parameter estimation further down the pipeline, it is useful if the statistical properties of the power spectrum estimates are simple and easy to calculate. The simplest case (which often occurs with the pixelized methods described below) is that where the data set is a multivariate Gaussian, described by the likelihood function of equation (1). Then the slowest step in the likelihood calculation is computing the determinant of the  $N \times N$  covariance matrix  $\mathbf{C}$ , for which the CPU time scales as  $N^3$ , so it is desirable to make the compressed data set as

small as is possible without losing information. It is also convenient if the statistical properties of the compressed data set, in particular, its covariance matrix, can be computed analytically. We will see that this is the case for the Karhunen-Loève and quadratic methods, but not for the maximum-likelihood method, where it requires numerical computation of the entire likelihood surface. Finally, the simplest covariance matrix one can desire is clearly one that is diagonal, *i.e.*, where the errors on the elements of the compressed data set are uncorrelated.

### 2.4. The wish list

In summary, the ideal data analysis/data compression method would

1. be lossless, at least for the parameters of interest,
2. give easy-to-compute and uncorrelated errors,
3. be computationally feasible in practice,
4. allow one to account for redshift-space distortions and systematic effects.

The first two items can be summarized by saying that we want the method to retain the cosmological information content of the original data set, distilled into a set of mutually exclusive (2) and collectively exhaustive (1) chunks.

## 3. POWER SPECTRUM ESTIMATION METHODS — AN OVERVIEW

In this section, we review the various methods for power spectrum estimation that have been proposed in the literature and present various extensions. We start in Section 3.1 with developing a formalism that is common to all our approaches. In Section 3.2, we discuss how the data might be discretized; that is, different ways of packaging the data into a convenient form  $\mathbf{x}$ . We then discuss various methods of power spectrum estimation: traditional methods which take the square of the amplitude of the Fourier modes (Section 3.3), the method of brute force likelihood (Section 3.4), the linear Karhunen-Loève method (Section 3.5), and a new quadratic method (Section 3.6). Our suggested approach to power spectrum estimation involves a combination of these methods in different regimes, as summarized in Figure 1, and described in more detail in Section 7.

### 3.1. Density field, shot noise and window functions

Following Peebles (1980), we model the observed galaxy distribution as a 3D Poisson process  $n(\mathbf{r}) = \sum_i \delta^D(\mathbf{r} - \mathbf{r}_i)$  with intensity  $\lambda(\mathbf{r}) = \bar{n}(\mathbf{r})[1 + \delta_r(\mathbf{r})]$ , where  $\delta_r$  is the underlying density field, not to be confused with the Dirac delta function  $\delta^D$ . The function  $\bar{n}$  is the selection function of the galaxy survey under consideration, *i.e.*,  $\bar{n}(\mathbf{r})dV$  is the expected (not the observed) number of galaxies in a volume  $dV$  about  $\mathbf{r}$  in the absence of clustering. The density fluctuations  $\delta_r$  are modeled as a homogeneous and isotropic (but not necessarily Gaussian) random field with power spectrum  $P(k)$ , and the power spectrum estimation problem is to estimate  $P(k)$  given a realization of  $n(\mathbf{r})$ .

With the exception of the brute force maximum likelihood technique, all of the methods described below compute band power estimates  $q_i$  that are quadratic functions

of the density field  $n$ , which means that they can be written as

$$q_i = \int \int E_i(\mathbf{r}, \mathbf{r}') \frac{n(\mathbf{r})}{\bar{n}(\mathbf{r})} \frac{n(\mathbf{r}')}{\bar{n}(\mathbf{r}')} d^3r d^3r' = \sum_{\alpha, \beta} \frac{E_i(\mathbf{r}_\alpha, \mathbf{r}_\beta)}{\bar{n}(\mathbf{r}_\alpha) \bar{n}(\mathbf{r}_\beta)} \quad (3)$$

for some pair weighting functions  $E_i$  which are designed to isolate different ranges of wavenumber  $k$  — the methods simply differ in their choices of  $E_i$ . Taking the expectation value of  $n(\mathbf{r})n(\mathbf{r}')/\bar{n}(\mathbf{r})\bar{n}(\mathbf{r}')$  produces three terms: “1” from the mean density,  $\delta^D(\mathbf{r}-\mathbf{r}')/\bar{n}(\mathbf{r})$  from shot noise and  $\delta_r(\mathbf{r})\delta_r(\mathbf{r}')$  from density fluctuations. By a derivation analogous to FKP and T95, one finds that these three terms give

$$\langle q_i \rangle = (2\pi)^3 W_i(\mathbf{0}) + b_i + \int W_i(\mathbf{k}) P(k) d^3k, \quad (4)$$

where  $W_i$ , the three-dimensional *window functions*, are given by

$$W_i(\mathbf{k}) = \hat{E}_i(\mathbf{k}, \mathbf{k}) \quad (5)$$

and

$$\hat{E}_i(\mathbf{k}, \mathbf{k}') \equiv \frac{1}{(2\pi)^3} \int E_i(\mathbf{r}, \mathbf{r}') e^{-i\mathbf{k}\cdot\mathbf{r}} e^{i\mathbf{k}'\cdot\mathbf{r}'} d^3r d^3r' \quad (6)$$

is a Fourier transform of  $E_i$ . We will often find it convenient to rewrite the last term of equation (4) as  $\int_0^\infty W_i(k) P(k) dk$ , where the *one-dimensional* window function is the angular average

$$W_i(k) = k^2 \int W_i(\mathbf{k}) d\Omega_k. \quad (7)$$

The *shot noise bias*, is given by

$$b_i \equiv \int \frac{E_i(\mathbf{r}, \mathbf{r})}{\bar{n}(\mathbf{r})} d^3r. \quad (8)$$

Alternatively,  $b_i$  can be made to vanish by omitting the terms with  $\alpha = \beta$  from the double sum in equation (3), as described in Appendix A. The term  $(2\pi)^3 W_i(\mathbf{0})$  simply probes the mean density of the survey, and as described in Section 5 and Appendix B, the functions  $E_i$  should always be chosen such that this term vanishes, *i.e.*, so that  $\int E_i(\mathbf{r}, \mathbf{r}') d^3r d^3r' = 0$ , thereby immunizing the power estimates to errors in normalization of  $\bar{n}$  (Section 5.1)<sup>2</sup>. The desirability of choosing windows with this property was first explicitly pointed out by Fisher *et al.* (1993), and this prescription was used also by *e.g.* Hamilton (1992) and Cole, Fisher & Wienberg (1994). We want to interpret  $q_i$  in equation (4) as probing a weighted average of the power spectrum, with the window function giving the weights, so  $E_i$  should be normalized so that  $W_i(k)$  integrates to unity. Using equation (5) and Parseval’s theorem, this gives

$$1 = \int_0^\infty W_i(k) dk = \int W_i(\mathbf{k}) d^3k = \int E_i(\mathbf{r}, \mathbf{r}) d^3r, \quad (9)$$

so if we think of  $E_i$  as a matrix, this normalization condition is simply  $\text{tr}[E_i] = 1$ . The window function has a simple geometrical interpretation (Hamilton 1997a). Rewriting equation (7) as

$$W_i(k) = \frac{4\pi k^2}{(2\pi)^3} \int_0^\infty w_i(r) j_0(kr) dr, \quad (10)$$

<sup>2</sup>In fact, the stronger constraint  $\int E_i(\mathbf{r}, \mathbf{r}') d^3r' = 0$  for all  $\mathbf{r}$  should be enforced, as discussed in Appendix B.

where

$$w_i(d) = \int \int E_i(\mathbf{r}, \mathbf{r}') \delta^D(|\mathbf{r} - \mathbf{r}'| - d) d^3r d^3r' \quad (11)$$

is the distribution of pair separations, we see that the only aspect of  $E_i$  that affects the window function is the weight given to different pair separations.

A special case is that where  $E_i$  is of rank one, *i.e.*, of the separable form

$$E_i(\mathbf{r}, \mathbf{r}') = \psi_i(\mathbf{r}) \psi_i(\mathbf{r}')^* \quad (12)$$

for some  $\psi_i$ . In this case, the last term in equation (3) can be written as  $|x_i|^2$ , where  $x_i$  is defined by equation (14) below, and the window function becomes simply

$$W_i(\mathbf{k}) = \frac{1}{(2\pi)^3} |\hat{\psi}_i(\mathbf{k})|^2. \quad (13)$$

(Here and throughout, hats denote Fourier transforms;  $\hat{\psi}(\mathbf{k}) \equiv \int e^{-i\mathbf{k}\cdot\mathbf{r}} \psi(\mathbf{r}) d^3r$  — see Appendix D.) We will see that both the traditional methods (Section 3.3) and the KL method (Section 3.5) are of this separable form, while the quadratic method that we present in Section 3.6 is not.

### 3.2. Pixelization

Hamilton (1997a) has recently derived the functions  $E_i$  that provide the minimum-variance power spectrum estimates for an arbitrary selection function and survey geometry. Unfortunately, this optimal weighting scheme is in general impractical to implement numerically, as it involves a computationally cumbersome infinite series expansion — only in the small-scale limit does it become simple, as will be described in Section 4.3. To proceed numerically, it is therefore convenient to discretize the problem. This reduces it to one similar to that of cosmic microwave background (CMB) experiments: estimating a power spectrum given noisy fluctuation measurements in a number of discrete “pixels”. Once the pixelization is done, the remaining steps are quite analogous to the CMB case (T97), and involve mere matrix operations such as inversion and diagonalization. These operations can often be further simplified by a more suitable choice of pixelization.

Let us define the overdensity in  $N$  “pixels”  $x_1, \dots, x_N$  by

$$x_i \equiv \int \left[ \frac{n(\mathbf{r})}{\bar{n}(\mathbf{r})} - 1 \right] \psi_i(\mathbf{r}) d^3r \quad (14)$$

for some set of functions  $\psi_i$ . We discuss specific choices of  $\psi_i$  in some detail below. One generally strives either to make these functions fairly localized in real space (in which case the pixelization is a generalized form of counts in cells) or fairly localized in Fourier space (in which case we will refer to the functions  $\psi_i$  as “modes” and to  $x_i$  as expansion coefficients). The “−1” term in equation (14) simply subtracts off the mean density. As we discuss in

Section 5 and Appendix B, one can and should choose the weight functions  $\psi_i$  to have zero mean, making this term irrelevant. This corresponds to requiring that

$$\int \psi_i(\mathbf{r}) d^3r = 0. \quad (15)$$

Let us group the pixels  $x_i$  into an  $N$ -dimensional vector  $\mathbf{x}$ . From equations (14) and (15) and a generalization of the derivation of equation (4), T95 shows that

$$\langle \mathbf{x} \rangle = \mathbf{0}, \quad (16)$$

$$\langle \mathbf{x}\mathbf{x}^\dagger \rangle = \mathbf{C} \equiv \mathbf{N} + \mathbf{S}, \quad (17)$$

where the shot noise covariance matrix is given by

$$\mathbf{N}_{ij} = \int \frac{\psi_i(\mathbf{r})\psi_j(\mathbf{r})^*}{\bar{n}(\mathbf{r})} d^3r \quad (18)$$

and the signal covariance matrix is

$$\mathbf{S}_{ij} = \frac{1}{(2\pi)^3} \int \hat{\psi}_i(\mathbf{k})\hat{\psi}_j(\mathbf{k})^* P(k) d^3k. \quad (19)$$

How should we choose our  $\psi_i$ 's to pixelize space? For a pixelization to be useful, we clearly want the data set  $\mathbf{x}$  to retain as large a fraction as possible of the cosmological information from the original data set (the galaxy positions), while simultaneously simplifying subsequent calculations. We here list several natural options, most of which have appeared in the literature.

### 3.2.1. Counts in cells

Here one partitions the survey volume into  $N$  mutually exclusive and collectively exhaustive volumes  $V_i$ , and defines  $\psi_i(\mathbf{r}) = \bar{n}(\mathbf{r})$  if  $\mathbf{r} \in V_i$ ,  $\psi_i(\mathbf{r}) = 0$  elsewhere. Thus  $x_i$  is simply the number of galaxies observed in  $V_i$ , minus the expected average. A set of useful approximations for computing  $\mathbf{N}$  and  $\mathbf{S}$  for this case is derived in VS96. To keep the number of cells from becoming intractably large, one might choose the cells to be larger in distant and poorly sampled regions of space than nearby.

With these sharp-edged cells, any linear combinations of pixels will correspond to a weight function that is discontinuous at cell boundaries. To avoid power leakage problems that this can in principle cause, one might use cells with “fuzzy” boundaries instead, for instance Gaussians as described in T95.

One can greatly simplify the computation of the covariance matrix by choosing all cells to have the same shape and to be spherically symmetric (*e.g.*, spheres or Gaussians), since in the absence of redshift-space distortions, the resulting  $\mathbf{S}_{ij}$  will depend only on the separation of the pixel centers and this correlation function can be pre-computed and splined once and for all. For the volume-limited case ( $\bar{n}$  constant), performing the appropriate integrals for identical spherical cells of radius  $R$ , separated by  $uR$ , gives

$$\mathbf{N}_{ij} = \begin{cases} \frac{(2-u)^2(4+u)}{16} \bar{n}V & \text{if } u < 2, \\ 0 & \text{if } u \geq 2, \end{cases} \quad (20)$$

<sup>3</sup>For the reader wishing to implement this pixelization in practice, the most efficient way to cover space with identical spheres is with face-centered cubic packing, which corresponds to centering a sphere at exactly half of all vertices of a cubic grid ( $l, m, n$ ) $a$  — for example, at those grid points where the integer sum  $l, m, n$  is even. All points will belong to at least one sphere if the sphere radius is chosen to equal the grid spacing  $a$ , and the average point will be covered by  $2\pi/3 \approx 2.1$  pixels, whereas a simple cubic grid gives  $\sqrt{3}\pi/2 \approx 2.7$ . Here  $\mathbf{N}_{ij}/\mathbf{N}_{ii} = 1 - 5/\sqrt{32} \approx 12\%$  for the 12 nearest neighbors of pixel  $i$ , zero for all other  $j \neq i$ .

where  $V = 4\pi R^3/3$ .<sup>3</sup>

### 3.2.2. Fourier modes

All of the above-mentioned pixels were fairly well-localized in real space. To make pixels reasonably localized in Fourier space, one can choose modes  $\psi_i$  that are plane waves, tapered by some weight function  $\phi$  to make them square integrable:

$$\psi_i(\mathbf{r}) = \phi(\mathbf{r})e^{i\mathbf{k}_i \cdot \mathbf{r}} \quad (21)$$

for some grid points  $\mathbf{k}_i$  in Fourier space. Choosing all modes that are periodic in a box containing the survey volume will ensure that this is a complete set, although some high-frequency cutoff is of course necessary to keep the number of pixels finite. Four different choices of the volume weighting function  $\phi$  have appeared in the literature:

$$\phi(\mathbf{r}) \propto \begin{cases} 1 & \text{inside survey volume} \\ 0 & \text{outside survey volume} \end{cases} \quad (22)$$

$$\phi(\mathbf{r}) \propto \bar{n}(\mathbf{r}) \quad (23)$$

$$\phi(\mathbf{r}) \propto \frac{\bar{n}(\mathbf{r})}{1 + \bar{n}(\mathbf{r})P} \quad (24)$$

$$\phi(\mathbf{r}) \propto \text{eigenfunction of } \left[ \nabla^2 - \frac{\gamma}{\bar{n}(\mathbf{r})} \right] \quad (25)$$

All are to be normalized so that the corresponding window functions integrate to unity; equation (9) implies equation (28) below. Note that without careful choice of the  $\mathbf{k}_i$ 's, equation (15) will *not* be satisfied in general for these pixelizations. The first choice, which weights all volume elements in the survey equally, was employed by *e.g.* Vogelely *et al.* (1992), Fisher *et al.* (1993), and Park *et al.* (1994). The second choice is used when determining the angular power spectrum of a sample without redshifts, *e.g.*, the APM survey (Baugh & Efstathiou 1994). Then all galaxies by default receive equal weight (moreover, modes can of course only be computed in the directions perpendicular to the line of sight). The third choice, advocated by Feldman, Kaiser & Peacock (1994, hereafter FKP), minimizes the variance in the limit when  $k^{-1} \ll$  the depth of the survey and is discussed in detail in Section 4.3.1. Here  $P$  denotes an *a priori* guess of the power in the band under consideration. The fourth choice (Tegmark 1995, hereafter T95), gives the narrowest window function for a given variance, where the constant  $\gamma$  determines the trade-off.

### 3.2.3. Spherical harmonic modes

The spherical wave choice

$$\psi_i(\mathbf{r}) = Y_{\ell m}(\hat{\mathbf{r}})j_\ell(k_n r), \quad (26)$$

where  $Y_{\ell m}$  is a spherical harmonic and  $j_\ell$  a spherical Bessel function, is well-suited for full-sky redshift surveys, and has the advantage (Fisher, Sharf, & Lahav 1994; Heavens & Taylor 1995) of greatly simplifying inclusion of the effect of redshift-space distortions in the analysis.

### 3.2.4. Guessed eigenmodes

In Section 3.5.1, we describe a set of smooth functions known as continuum signal-to-noise eigenmodes. These modes have a number of useful properties. In particular, there is an integer  $N$  such that the first  $N$  eigenmodes retain virtually all the cosmological information in the survey. If one has a reasonable *a priori* guess as to the shape of these functions (given that they depend on the survey geometry), the first  $N$  of these guessed modes are obviously a good choice for the pixelization functions  $\psi_i$ , since the amount of information destroyed by the pixelization process will then be small.

### 3.3. Traditional methods

The traditional approach has been to estimate the power by simply squaring the pixels ( $q_i = |x_i|^2$ ), choosing the pixels to be Fourier modes as described above. This corresponds to the pair weighting of equation (12), where  $\psi_i$  is given by equation (21) and  $\phi$  is specified by equation (22), (23), (24) or (25). Equation (4) shows that

$$\langle q_i \rangle = \hat{\phi}(\mathbf{0})^2 + \int \frac{\phi(\mathbf{r})^2}{\bar{n}(\mathbf{r})} d^3r + \frac{1}{(2\pi)^3} \int |\hat{\phi}(\mathbf{k} - \mathbf{k}_i)|^2 P(\mathbf{k}) d^3k, \quad (27)$$

the last term of which is simply the true power spectrum convolved with the function  $|\hat{\phi}(\mathbf{k})|^2/(2\pi)^3$ . The 3D window function is thus  $W_i(\mathbf{k}) = |\hat{\phi}(\mathbf{k} - \mathbf{k}_i)|^2/(2\pi)^3$ . Using this and Parseval's theorem (or equation (9) directly), one finds that the window function normalization constraint  $\int W_i(\mathbf{k}) d^3k = 1$  corresponds to simply

$$\int \phi(\mathbf{r})^2 d^3r = 1. \quad (28)$$

These simple expressions have frequently been used in the literature, but an annoying complication has often been neglected. As described in Section 5, the fact that the normalization of  $\bar{n}$  is not known *a priori*, but is determined from the observed galaxies (the integral constraint problem) can be eliminated by choosing weight functions  $\psi_i$  that are orthogonal to the monopole, *i.e.*, such that  $\hat{\psi}_i(\mathbf{0}) = 0$ . Although this is easy to arrange with the pixelized methods described below, the choice of equation (21) does generally *not* have this important property. To obtain a correct answer with the traditional methods, this must be corrected for. As shown in Appendix B, the power estimator

$$\tilde{P}_i \equiv \left[ \frac{|x_i|^2 - b_i}{A_i} \right] \quad (29)$$

is unbiased and incorporates the integral constraint correction (when  $\bar{n}$  is normalized so that  $x_i = 0$  for  $\mathbf{k}_i = \mathbf{0}$ ) if the normalization factor  $A_i$  and the shot noise correction  $b_i$  are given by

$$A_i = \left( 1 + \left| \frac{\hat{\phi}(\mathbf{k}_i)}{\hat{\phi}(\mathbf{0})} \right|^2 \right) a(\mathbf{0}) - 2 \operatorname{Re} \left\{ \frac{\hat{\phi}(\mathbf{k}_i)}{\hat{\phi}(\mathbf{0})} a(\mathbf{k}_i) \right\}, \quad (30)$$

$$b_i = \left( 1 + \left| \frac{\hat{\phi}(\mathbf{k}_i)}{\hat{\phi}(\mathbf{0})} \right|^2 \right) b(\mathbf{0}) - 2 \operatorname{Re} \left\{ \frac{\hat{\phi}(\mathbf{k}_i)}{\hat{\phi}(\mathbf{0})} b(\mathbf{k}_i) \right\}, \quad (31)$$

where the functions  $a$  and  $b$  are defined by

$$a(\mathbf{k}) \equiv \int \phi(\mathbf{r})^2 e^{i\mathbf{k} \cdot \mathbf{r}} d^3r, \quad (32)$$

$$b(\mathbf{k}) \equiv \int \frac{\phi(\mathbf{r})^2}{\bar{n}(\mathbf{r})} e^{i\mathbf{k} \cdot \mathbf{r}} d^3r. \quad (33)$$

If the survey is volume limited, then  $\bar{n}$  is independent of  $\mathbf{r}$ ,  $b(\mathbf{k}) = a(\mathbf{k})/\bar{n}$ , and  $b_i = A_i/\bar{n}$ .

After computing power estimates  $q_i$  at a large grid of points  $\mathbf{k}_i$ , one finally takes some weighted averages of the  $q_i$  to obtain power estimates in some bands of (scalar)  $k$  ( $= |\mathbf{k}|$ ). The problem of finding the weights that minimize the variance of the band power estimators is unfortunately quite a difficult one, and in general involves solving a numerically unpleasant quadratic programming problem (T95). For this reason, the customary approach has been to simply give all  $q_i$  equal weights in some spherical shells in  $\mathbf{k}$ -space although, as described in VS96, this is in general far from optimal.

### 3.4. Brute force likelihood method

Let us parametrize the power spectrum  $P(k)$  by some parameter vector  $\Theta$  as in Section 2.1. In the approximation that the probability distribution for the pixel vector  $\mathbf{x}$  is a multivariate Gaussian, it is given by equation (1) with mean  $\mathbf{m} = \mathbf{0}$ . The *maximum likelihood estimator* of  $\Theta$ , denoted  $\Theta_{ml}$ , is simply that  $\Theta$ -vector that maximizes the likelihood  $f(\mathbf{x}; \Theta)$ . This maximization problem can unfortunately not be solved analytically when the number of pixels exceeds one, so  $\Theta_{ml}$  is a complicated non-linear function of  $\mathbf{x}$  that must be computed by solving the maximization problem numerically. Since one generally wants error bars on the estimate as well, one typically evaluates the likelihood function at a dense grid of points in parameter space and rescales it to integrate to unity. These final results are often illustrated in contour plots, as at the bottom of Figure 1.

### 3.5. Linear (Karhunen-Loève) method

As will be discussed in Section 6, the traditional methods generally destroy information, while the brute force method is lossless but computationally impractical. The Karhunen-Loève (KL) method (Karhunen 1947) maintains the advantage of the brute-force method (indeed, it can produce the identical answer faster), and has additional useful features as well, as we detail below. It was first introduced into Large-Scale Structure analysis by Vogeley & Szalay (see VS96), and it has also been successfully applied to Cosmic Microwave Background data (*e.g.* Bunn 1995; Bond 1995; TTH; Jaffe, Knox, & Bond 1997). We start by defining signal-to-noise eigenmodes in Section 3.5.1, before generalizing the technique in Section 3.5.2.

#### 3.5.1. Signal-to-noise eigenmodes

The signal-to-noise eigenmode method consists of defining a new data vector

$$\mathbf{y} \equiv \mathbf{B}\mathbf{x}, \quad (34)$$

where  $\mathbf{b}$ , the rows of the matrix  $\mathbf{B}$ , are the  $N$  eigenvectors of the generalized eigenvalue problem

$$\mathbf{S}\mathbf{b} = \lambda \mathbf{N}\mathbf{b}, \quad (35)$$

sorted from highest to lowest eigenvalue  $\lambda$  and normalized so that  $\mathbf{b}^t \mathbf{N} \mathbf{b} = \mathbf{I}$ . This implies that

$$\langle y_i y_j \rangle = \delta_{ij} (1 + \lambda_i), \quad (36)$$

which means that the transformed data values  $\mathbf{y}$  have the desirable property of being *statistically orthogonal*, *i.e.*, uncorrelated. In the approximation that the distribution function of  $\mathbf{x}$  is a multivariate Gaussian, this also implies that they are statistically independent — then  $\mathbf{y}$  is merely a vector of independent Gaussian random variables. Moreover, since the eigenmodes diagonalize both  $\mathbf{S}$  and  $\mathbf{N}$  simultaneously, equation (35) shows that the eigenvalues  $\lambda_i$  can be interpreted as a signal-to-noise ratio  $\mathbf{S}/\mathbf{N}$ . Since equation (36) shows that the quantity  $y_i^2 - 1$  on average equals this signal-to-noise ratio, it is a useful band power estimator when normalized so that its window function integrates to unity. The window function is given by equation (13) with  $\psi_i$  replaced by the continuous KL mode defined by

$$\psi'_i(\mathbf{r}) \equiv \sum_{j=1}^N \mathbf{B}_{ij} \psi_j(\mathbf{r}), \quad (37)$$

since  $y_i = \int [n(\mathbf{r})/\bar{n}(\mathbf{r}) - 1] \psi'_i(\mathbf{r}) d^3r$ . For the volume-limited case, the noise power is simply  $1/\bar{n}$ , so the correctly normalized and bias-corrected KL band power estimators are simply “signal = noise  $\times$  signal-to-noise”, *i.e.*,

$$q_i \equiv \frac{y_i^2 - 1}{\bar{n}}; \quad (38)$$

compare this with equation (29). Since the matrix  $\mathbf{B}$  is invertible, the final data set  $\mathbf{y}$  clearly retains all the information that was present in  $\mathbf{x}$ . In summary, the KL transformation partitions the information content of the original data set  $\mathbf{x}$  into  $N$  chunks that are

1. mutually exclusive (independent),
2. collectively exhaustive (jointly retaining all the information), and
3. sorted from best to worst in terms of their information content.

Typically, most of the KL coefficients  $y_i$  have a signal-to-noise ratio  $\lambda \ll 1$ , so that the bulk of the cosmological information is retained in the first  $N'$  coefficients,  $N' \ll N$ , which is why the KL method is often referred to and used as *data compression*. One can thus throw away all but the first  $N'$  numbers  $y_i$  without any appreciable information loss, and this compressed data set will still satisfy properties 1 and 3 exactly, and 2 to a good approximation.

Bunn (1995) and VS96 have pointed out that the  $\mathbf{S}/\mathbf{N}$ -coefficients  $\mathbf{y}$  are useful for power spectrum estimation since as long as the galaxy survey probes only scales smaller than the peak in the power spectrum (*cf.*, the discussion in Section 6.3.3), the first  $N'$  window functions  $W_i$  have the following two properties:

1. They are narrow in  $k$ -space,

2. As  $i$  increases from 1 to  $N'$ , they probe all the scales accurately measured by the survey, from largest to smallest.

Since they are also uncorrelated, these power spectrum estimators therefore have all desirable properties that one may wish for: they distill the cosmological information content of the data set into a set of mutually exclusive and collectively exhaustive chunks, which correspond to the band powers in a set of narrow bands. In the approximation that  $\mathbf{y}$  has a Gaussian distribution, the probability distributions of the power estimates  $q_i$  are simple: they are independent  $\chi^2$  distributions with one degree of freedom.<sup>4</sup>

### 3.5.2. General KL modes

Let us write  $\mathbf{C} = \theta_i \mathbf{S} + \mathbf{N}$ , where the power spectrum normalization parameter  $\theta_i = 1$  in the fiducial model. Since  $\mathbf{S} = \mathbf{C}_{,i} \equiv \partial \mathbf{C} / \partial \theta_i$ , equation (35) can be rewritten as (TTH)

$$\mathbf{C}_{,i} \mathbf{b} = \lambda' \mathbf{C} \mathbf{b}, \quad (39)$$

where  $\lambda' = \lambda / (1 + \lambda)$  or, equivalently,  $\lambda = \lambda' / (1 - \lambda')$ . From now on, we will normalize the eigenvectors so that  $\mathbf{b}^t \mathbf{C} \mathbf{b} = 1$  instead of  $\mathbf{b}^t \mathbf{N} \mathbf{b} = 1$ , since this is more convenient throughout the rest of the paper. The matrix elements  $\mathbf{B}_{ij}$  are thus a factor  $(1 + \lambda_i)^{1/2}$  smaller than in the previous subsection. As shown in TTH, solving the eigenvalue equation (39) is useful for *any* parameter  $\theta_i$  on which  $\mathbf{C}$  depends, even those which do not affect only the power spectrum (*e.g.*, redshift-space distortions, *cf.*, Appendix C), and the signal-to-noise eigenmode method discussed above is just the special case where  $\theta_i$  is the power normalization. The three properties listed above continue to hold in the general case, and the “information content” in item 3 above now refers to the information about the parameter  $\theta_i$ .

The KL method is a very general data analysis tool. Note that the eigenmodes continue to be mutually exclusive and collectively exhaustive if we replace  $\mathbf{C}_{,i}$  by *any* symmetric matrix  $\mathbf{M}$  in equation (39). To ensure that the KL modes give narrow window functions ranging from small to large  $k$ , one can therefore choose  $\mathbf{M}$  to be the signal covariance matrix  $\mathbf{S}$  that would arise from some monotonically decreasing power spectrum, for instance  $P(k) \propto k^{-3}$ . In that case, the modes become sorted not by how much information they contain on  $\theta_i$ , but by the ratio of wavelength to noise, essentially the scale that they probe. We discuss this point further in Section 6.3.3.

### 3.5.3. KL modes are asymptotically pixelization-independent

The pixelizations listed in Section 3.2 were all in some sense arbitrary, and generally somewhat redundant. The KL modes can eliminate this arbitrariness, as mentioned in Section 3.2.4. If the pixelization functions  $\psi_i$  formed a complete set, spanning the space of all square-integrable functions over the survey volume, the continuum KL modes defined by equation (37) would be some smooth functions  $\psi'_i(\mathbf{r})$  that were independent of the pixelization used to compute them and depended only on  $P(k)$ ,  $\bar{n}(\mathbf{r})$  and the geometry of the survey. In practice, the functions

<sup>4</sup>To prevent power spectrum plots from becoming too cluttered with points with large error bars, it is convenient to combine neighboring band power estimates with a weighted average — these broader band powers will of course still be uncorrelated since all the  $q_i$  are.

$\psi_i$  do of course not form a complete set, since one is limited to a finite number of pixels, but the continuum KL modes  $\psi'_i(\mathbf{r})$  can nonetheless be computed numerically. By choosing a pixelization that can resolve all features down to some scale  $R$ , equation (37) will accurately approximate all continuum modes whose window functions  $W_i(k)$  probe only scales  $k^{-1} \gg R$ . If the number of pixels are increased further to probe smaller scales, the first  $N'$  modes remain stable against this perturbation: the first  $N'$  eigenvalues and eigenvectors would only change by a small amount (Szalay & Vogeley 1997). The new modes, on the other hand, would represent the small scale noise probed by the new pixel scale. By using the functions  $\psi'_i(\mathbf{r})$  to pixelize the data,  $i = 1, \dots, N$ , one can thus make sure that all of the cosmological signal down to the scale probed by  $\psi'_N$  is retained.

#### 3.5.4. Using KL modes for trouble spotting

If the assumed power spectrum model is correct, the KL coefficients  $y_i$  defined by equation (34) will be independent Gaussian random variables with zero mean and unit variance. This offers an efficient way of testing whether the data are inconsistent with this model. The detection of, say, a  $6-\sigma$  outlier ( $|y_i| > 6$ ) would provide strong evidence that there is either more variance on the scale probed by the  $i^{\text{th}}$  mode than the fiducial power spectrum assumed, or that the probability distribution is strongly non-Gaussian on that scale. Even if it goes undetected, an incorrect assumed model does not bias the estimate of the power spectrum, as discussed below in Section 6.3.5.

#### 3.5.5. Using KL modes for linear filtering

The KL eigenmodes have an additional use. The process of throwing away the eigenmodes with low signal-to-noise ratios splits the space of all possible density fields given the data into two — one subspace that mostly contains noise, and one that is dominated by our generalized signal. The two are statistically orthogonal to one another. The expansion of a given dataset over the signal subspace will substantially reduce the noise, thus representing a useful linear filtering of the data. Since it maximizes the signal for a given number of included modes, the KL transform is sometimes referred to as “optimal subspace filtering”. More generally, let us define a filtered data set

$$x'_i \equiv \sum_{j=1}^N (\mathbf{C}\mathbf{B}^t)_{ij} w_j y_j \quad (40)$$

for some weights  $w_j$ . The generalized eigenvector orthogonality relation gives  $\mathbf{B}\mathbf{C}\mathbf{B}^t = \mathbf{I}$  (cf., VS96, TTH), which implies that  $\mathbf{C}^{-1} = \mathbf{B}^t\mathbf{B}$  and  $\mathbf{C}\mathbf{B}^t\mathbf{B} = \mathbf{I}$ . Hence equation (34) gives  $\mathbf{C}\mathbf{B}^t\mathbf{y} = \mathbf{x}$ , which implies that we recover the original data set ( $\mathbf{x}' = \mathbf{x}$ ) in equation (40) if we choose the weights  $w_j = 1$ . Another simple example is the optimal subspace filtering mentioned above, which corresponds to the choice  $w_j = 1$  for  $j \leq N'$ ,  $w_j = 0$  otherwise. Finally, it is easy to show that the choice  $w_j = \lambda'_j$  gives *Wiener filtering*, which is defined by  $\mathbf{x}' = \mathbf{S}\mathbf{C}^{-1}\mathbf{x}$ . In other words, Wiener filtering becomes diagonal in the KL basis, since it diagonalizes  $\mathbf{S}$  and  $\mathbf{C}$  simultaneously. Indeed, Wiener filtering is but one of many linear filters that are straightforward to implement in the KL basis.

### 3.6. Quadratic method

In both traditional methods and the pixelized KL technique, the power spectrum estimates  $q_i$  are some quadratic functions of the observed density field  $n(\mathbf{r})$ , *i.e.*, of the form given by equation (3). Hamilton (1997a) adopted a more ambitious approach, and computed the unbiased quadratic power estimators that have minimal variance, using a series expansion. T97 subsequently showed that these estimators are unbeatable; their Fisher information matrix is identical to that of the raw data, so no non-quadratic unbiased estimators can give smaller variance. Moreover, they can be computed without recourse to the numerically cumbersome series expansion of Hamilton 1997a (c.f. T97 and Knox, Bond, & Jaffe 1997 for applications to CMB observations). Here we show how this method can be applied to galaxy surveys, and its relation to the KL method.

We specify a set of  $N'$  band powers  $p_i$  by

$$k_i \leq k \leq k_{i+1}, \quad \text{where } 0 = k_1 < k_2 < \dots < k_{N'+1} = \infty, \quad (41)$$

and group them into an  $N'$ -dimensional vector  $\mathbf{p}$ . For the method to be strictly lossless, these bands should be chosen to be quite narrow compared to the scales on which the power spectrum varies. One first computes a compressed data vector  $\mathbf{q}$  whose  $N'$  elements are quadratic functions of the data set  $\mathbf{x}$ . These are defined by

$$q_i \equiv \frac{1}{2} \mathbf{z}^t \mathbf{C}_{,i} \mathbf{z}, \quad (42)$$

where the vector  $\mathbf{z}$  is given by

$$\mathbf{z} \equiv \mathbf{C}^{-1} \mathbf{x}, \quad (43)$$

and the matrix  $\mathbf{C}_{,i}$  is defined by

$$(\mathbf{C}_{,i})_{ab} \equiv \frac{1}{(2\pi)^3} \int_{k_i < |\mathbf{k}| < k_{i+1}} \hat{\psi}_a(\mathbf{k}) \hat{\psi}_b(\mathbf{k})^* d^3k. \quad (44)$$

That is,  $\mathbf{C}_{,i}$  is the derivative of the covariance matrix  $\mathbf{C}$  (equation (17)) with respect to the normalization of the  $i^{\text{th}}$  band, in the limit of narrow bands. Rewriting this as

$$q_i \equiv \frac{1}{2} \mathbf{x}^\dagger \mathbf{E}_i \mathbf{x}, \quad (45)$$

where

$$\mathbf{E}_i \equiv \mathbf{C}^{-1} \mathbf{C}_{,i} \mathbf{C}^{-1}, \quad (46)$$

we see that the matrix  $\mathbf{E}_i$  is simply a discrete version of the pair weighting function  $E_i(\mathbf{r}, \mathbf{r}')$  in equation (3). Note that it is not separable.

For the Gaussian case, the Fisher information matrix for  $\mathbf{p}$  defined by equation (2) reduces to (VS96, TTH)

$$\mathbf{F}_{ij} = \frac{1}{2} \text{tr} [\mathbf{C}^{-1} \mathbf{C}_{,i} \mathbf{C}^{-1} \mathbf{C}_{,j}], \quad (47)$$

and T97 shows that both the mean and the covariance of  $\mathbf{q}$  are given in terms of  $\mathbf{F}$ :

$$\langle \mathbf{q} \rangle = \mathbf{F} \mathbf{p}, \quad (48)$$

$$\langle \mathbf{q} \mathbf{q}^t \rangle - \langle \mathbf{q} \rangle \langle \mathbf{q} \rangle^t = \mathbf{F}. \quad (49)$$



This means that  $\mathbf{F}^{-1}\mathbf{q}$  is an optimal estimator of  $\mathbf{p}$ , since its covariance matrix is precisely the inverse of the Fisher matrix. Moreover, as shown in T97, compressing the data set  $\mathbf{x}$  into the coefficients  $\mathbf{q}$  for some sufficiently narrow bands is a strictly lossless procedure, retaining all the information about those cosmological parameters that affect galaxy clustering through the power spectrum alone. Equation (48) shows that, in terms of the band powers, the window functions  $W$  of equation (7) for the coefficients  $q_i$  are simply proportional to the rows of the ubiquitous Fisher matrix.

The coefficients  $\mathbf{F}^{-1}\mathbf{q}$  tend to be both correlated and noisy, and therefore it is better to work with the transformed coefficients defined by

$$\tilde{\mathbf{p}} \equiv \mathbf{F}^{-1/2}\mathbf{q}, \quad (50)$$

renormalized so that their window functions integrate to unity. Here  $\mathbf{F}^{1/2}$  denotes the symmetric matrix whose square is  $\mathbf{F}$  – it is readily computed by diagonalization. As shown by Tegmark & Hamilton (1997), these coefficients are all uncorrelated (multiply equation (49) on both the right and the left by  $\mathbf{F}^{-1/2}$  to see this), and moreover tend to be very well-behaved numerically, with narrow non-negative window functions (the rows of  $\mathbf{F}^{1/2}$ ) spanning the entire range of scales probed by the survey.

#### 4. RELATIONS BETWEEN THE METHODS

##### 4.1. Relation between KL and quadratic method

As we will now show, the linear and quadratic pixelized methods are closely related – the latter is simply a faster way of computing the same band power estimates.

Let us optimize our KL modes to estimate not the overall power normalization, but the band power in band  $j$ . As we showed in Section 3.5.5,

$$\mathbf{C}^{-1} = \mathbf{B}^t \mathbf{B}. \quad (51)$$

Introducing the diagonal matrix  $\mathbf{\Lambda} \equiv \text{diag}\{\lambda'_i\}$ , equation (39) implies that

$$\mathbf{B}\mathbf{C}_i\mathbf{B}^t = \mathbf{\Lambda}. \quad (52)$$

We are suppressing the index  $j$  here for simplicity, although the eigenvectors in  $\mathbf{B}$  and the eigenvalues in  $\mathbf{\Lambda}$  of course depend on which power band  $j$  we optimize for. Equations (34), (51) and (52) allow us to rewrite equation (42) as

$$\begin{aligned} 2q_i &= \mathbf{x}^\dagger \mathbf{C}^{-1} \mathbf{C}_i \mathbf{C}^{-1} \mathbf{x} = \mathbf{x}^\dagger \mathbf{B}^t \mathbf{B} \mathbf{C}_i \mathbf{B}^t \mathbf{B} \mathbf{x} \\ &= \mathbf{y}^t \mathbf{\Lambda} \mathbf{y} = \sum \lambda'_j y_j^2, \end{aligned} \quad (53)$$

*i.e.*, as a weighted average of the squared KL coefficients  $y_i$ , with weights given by the KL eigenvalues  $\lambda'_i$ . Thus the coefficients are weighted by their inverse variance, which means that this is the minimum-variance band power estimator based on the squared KL coefficients, so after subtracting off shot noise and normalizing correctly, the linear (KL) and quadratic methods give exactly the same estimator for the band power. As described in Section 6.4,

<sup>5</sup>An intuitive way to understand why all directions in  $k$ -space should receive equal weight when  $\Delta k \gg L^{-1}$  is to note that in this limit, the number of coherence volumes that fit into a given solid angle in the shell is independent of its shape (and hence independent of direction in  $k$ -space), being merely the ratio of the shell subvolume to the coherence volume.

the quadratic estimator is simply faster to compute. A more intuitive way of understanding why the two methods give the same result is to note that the quadratic method was derived explicitly to be the minimum variance estimator (T97; cf., equation (48)), and that VS96 showed that the KL approach is guaranteed to minimize the variance as well.

##### 4.2. Relation between quadratic and ML methods: iteration

If the quadratic method is repeated using the output (measured) power spectrum as the input (fiducial) power spectrum, then this iteration will eventually converge to the power spectrum that would be obtained with the brute force maximum-likelihood method (Knox 1997). This is because the quadratic method can be derived by expanding the logarithmic likelihood  $\ln f$  to second order around the fiducial point and maximizing it. The iteration thus seeks the maximum of  $\ln f$  by repeatedly approximating it with a parabola. This is essentially the maximum-gradient method for maximization, which is known to have excellent convergence properties. In the one-dimensional case, this is equivalent to finding the zero of  $(\ln f)'$  by repeated linear approximations. This is simply the Newton-Raphson root-finding method, known to converge exponentially fast and asymptotically double the number of correct decimals in each iteration.

It should be stressed that using a noisy measured power spectrum as fiducial spectrum when computing  $\mathbf{C}$  is not necessarily a good thing to do, since it neglects the commonly held belief that  $P(k)$  is a smooth function. This can produce misleadingly small error bars, as the following example illustrates. Suppose sample variance or a shot noise fluctuation makes a band power measurement ten times smaller than the true value. and this is used as the new fiducial band power  $P$  (prior). Then equation (61) shows that the nominal  $\Delta P$  will be ten times too small as well.

##### 4.3. Relation between quadratic and FKP methods: the small scale limit

For a traditional method with a volume weighting function  $\phi(\mathbf{r})$ , we define a quantity  $L$  implicitly by

$$\frac{1}{(2\pi)^3} \int_{kL < 1} |\hat{\phi}(\mathbf{k})|^2 d^3k = 1/2, \quad (54)$$

*i.e.*,  $L^{-1}$  is the radius of a sphere in Fourier space containing half of the  $\mathbf{k} = \mathbf{0}$  window function. For simple volumes such as a pencil beams, a slices or spheres,  $L$  is of the order of the width of the survey in its *narrowest* direction. We will now show that in the small-scale limit where  $k^{-1} \ll L$ , the quadratic method reduces to the FKP method, which implies that the latter is lossless and hence unbeatable for measuring the power spectrum on the smallest scales, as was pointed out by Hamilton (1997a).

##### 4.3.1. Derivation of the FKP method

The FKP method (Feldman, Kaiser & Peacock 1994) is the traditional method described in 3.3, using the volume weighting of equation (24). The rank one power estimates  $|x_a^2|$  are averaged with equal weights<sup>5</sup> for all modes in a

spherical shell  $|\mathbf{k}| = k_a$ , so integrating equation (12) over this shell using equation (21) for the pixels, we see that this corresponds to the pair weighting

$$E_i(\mathbf{r}, \mathbf{r}') = \phi(\mathbf{r})\phi(\mathbf{r}')j_0(k_i|\mathbf{r} - \mathbf{r}'|), \quad (55)$$

where  $j_0(x) \equiv \sin(x)/x$ . This holds for any choice of volume weighting function  $\phi$ . The specific FKP choice given by equation (24) is derived by minimizing the variance of the corresponding power estimators  $q_i$ . This involves a number of approximations. We summarize the derivation here, to clarify why the FKP weighting is optimal only on small scales.

Substituting equations (14) and (21) into equations (18) and (19), we obtain the pixel covariance matrix

$$\begin{aligned} \mathbf{C}_{ab} = & \frac{1}{(2\pi)^3} \int \hat{\phi}(\mathbf{k} - \mathbf{k}_a) \hat{\phi}(\mathbf{k} - \mathbf{k}_b)^* P(k) d^3k \\ & + \int e^{i(\mathbf{k}_a - \mathbf{k}_b) \cdot \mathbf{r}} \frac{\phi(\mathbf{r})^2}{\bar{n}(\mathbf{r})} d^3r. \end{aligned} \quad (56)$$

The function  $\hat{\phi}(\mathbf{k})$  roughly falls off on a scale  $L^{-1}$ . As long as  $L^{-1} \ll k$  and the power spectrum  $P(k)$  is a smooth function,  $P(k)$  will therefore be almost constant where the first integrand is non-negligible (*i.e.*, where  $|\mathbf{k} - \mathbf{k}_a| \lesssim L^{-1}$  and  $|\mathbf{k} - \mathbf{k}_b| \lesssim L^{-1}$ ) and can be approximately factored out of the  $k$ -integral. Using the convolution theorem, this yields

$$\mathbf{C}_{ab} \approx \int e^{i(\mathbf{k}_a - \mathbf{k}_b) \cdot \mathbf{r}} \phi(\mathbf{r})^2 \left[ P + \frac{1}{\bar{n}(\mathbf{r})} \right] d^3r, \quad (57)$$

where  $P \equiv P([k_a + k_b]/2)$ . This shows that  $\mathbf{C}_{ab} \approx 0$  if  $|\mathbf{k}_a - \mathbf{k}_b| \gg L^{-1}$ , so power estimates separated by much more than  $\Delta k = L^{-1}$  are essentially uncorrelated. Conversely, power estimates from nearby shells with  $|\mathbf{k}_a - \mathbf{k}_b| \ll L^{-1}$  are almost perfectly correlated and therefore redundant. The FKP method therefore averages the power estimates  $|x_a|^2$  in thicker shells  $|\mathbf{k}_a| \in [k_i, k_{i+1}]$  as in equation (41), whose widths satisfy  $L^{-1} \ll |k_{i+1} - k_i| \ll k$ , giving approximately uncorrelated power estimates  $q_i$ . This approximation clearly only holds for small scales,  $k^{-1} \ll L$ . We denote the volume of the  $i^{\text{th}}$  shell

$$V_s \equiv \frac{4}{3}\pi (k_{i+1}^3 - k_i^3). \quad (58)$$

Assuming that the pixelized data  $\mathbf{x}$  is Gaussian distributed, the variance of the power estimator  $q_i$  is simply given by averaging  $2|\mathbf{C}_{ab}|^2$  over the shell, *i.e.*,

$$(\Delta q_i)^2 = \frac{2}{V_s^2} \int \int |\mathbf{C}_{ab}|^2 d^3k_a d^3k_b, \quad (59)$$

where both integrals are to be taken over the  $i^{\text{th}}$  shell. Substituting equation (57), and using the fact that  $L^{-1} \ll |\mathbf{k}_a - \mathbf{k}_b| \ll k$ , one of these integrals simply produces a factor  $V_s$ . Applying Parseval's theorem to the result and

<sup>6</sup>Since  $kL \gg 1$ , equation (28) does not need the integral constraint correction.

<sup>7</sup>Since  $\mathbf{b} = \mathbf{A}\mathbf{x}$  means  $b_i = \sum_j \mathbf{A}_{ij}x_j$  in the discrete case and  $b(\mathbf{r}) = \int \mathbf{A}(\mathbf{r}, \mathbf{r}')x(\mathbf{r}')d^3r'$  in the continuous case, we see that matrix multiplication introduces units of the volume element, in this example  $d^3r$ . Thus the continuous analog of the identity matrix,  $\mathbf{I}(\mathbf{r}, \mathbf{r}') \equiv \delta^D(\mathbf{r} - \mathbf{r}')$ , is its own inverse, since  $(\mathbf{I}^2)(\mathbf{r}, \mathbf{r}') \equiv \int \mathbf{I}(\mathbf{r}, \mathbf{r}'')\mathbf{I}(\mathbf{r}'', \mathbf{r}')d^3r'' = \mathbf{I}(\mathbf{r}, \mathbf{r}')$ , even though it is not dimensionless — the delta function  $\delta^D$  has units of inverse volume.

using equation (28) to normalize<sup>6</sup> finally leaves us with the approximation

$$\left( \frac{\Delta q_i}{\langle q_i \rangle} \right)^2 \approx 2(2\pi)^3 \frac{\int \phi(\mathbf{r})^4 \left[ 1 + \frac{1}{\bar{n}(\mathbf{r})P} \right]^2 d^3r}{V_s \left[ \int \phi(\mathbf{r})^2 d^3r \right]^2}. \quad (60)$$

This holds for any weighting function  $\phi$ . The FKP choice of  $\phi$  is derived by minimizing this approximate expression for the variance. Since it is left unchanged if we multiply  $\phi$  by a constant, we can for simplicity impose the normalization constraint  $\int \phi^2 d^3r = 1$ . Minimizing the numerator of equation (60) with a Lagrange multiplier for this constraint now gives the FKP weighting of equation (24). Substituting this back into equation (60) and omitting the power band index  $i$  for simplicity finally yields

$$\left( \frac{\Delta P}{P} \right)^2 \equiv \left( \frac{\Delta q}{\langle q \rangle} \right)^2 \approx \frac{2(2\pi)^3}{V_s V^{\text{eff}}}, \quad (61)$$

where

$$V^{\text{eff}}(k) \equiv \int \left[ \frac{\bar{n}(\mathbf{r})P(k)}{1 + \bar{n}(\mathbf{r})P(k)} \right]^2 d^3r \quad (62)$$

can be interpreted as the *effective volume* probed, since the integrand is of order unity where one is signal dominated ( $P \gg 1/\bar{n}$ ) and  $\sim 0$  where one is noise dominated. For a volume-limited survey with spatial volume  $V$  and constant  $\bar{n}$ , the FKP prescription weights all galaxies equally, and we simply have  $V^{\text{eff}} = [1 + 1/\bar{n}P]^{-2}V$ . An intuitive way to understand equation (61) is to note that the nearby Fourier amplitudes  $x_i$  are correlated over a *coherence volume*  $V_c \sim (2\pi)^3/V$ . Thus as long as shot noise is not dominant,  $\Delta P/P \sim \sqrt{2/\mathcal{N}}$ , where  $\mathcal{N}$  is the number of approximately uncorrelated volumes  $V_c$  that fit into the shell volume  $V_s$ . In conclusion, we have shown that for traditional methods, the FKP volume weighting of equation (24) is optimal if and only if we limit ourselves to small scales,  $k^{-1} \ll L$ .

#### 4.3.2. The small-scale limit of the quadratic method

It is often convenient to work in the continuum limit where a discrete index  $i$  is replaced by a continuous variable such as  $\mathbf{r}$  or  $\mathbf{k}$ . Vectors  $a_i$  and matrices  $\mathbf{A}_{ij}$  then correspond to functions of one and two variables, such as  $a(\mathbf{r})$  and  $A(\mathbf{r}, \mathbf{r}')$ . Since all sums get replaced by integrals in this limit, units frequently differ from the discrete case<sup>7</sup>.

Let us take the pixelization functions to be Dirac delta functions  $\psi_i(\mathbf{r}) \equiv \delta^D(\mathbf{r} - \mathbf{r}_i)$ , corresponding to a continuum of pixels

$$x(\mathbf{r}) = \frac{n(\mathbf{r})}{\bar{n}(\mathbf{r})} - 1, \quad (63)$$

and choose our parameters to be the values of the 3D power spectrum:

$$\theta_i = P(\mathbf{k}_i). \quad (64)$$

The matrices  $\mathbf{C}$  and  $\mathbf{C}_{,i}$  then reduce to

$$\mathbf{C}(\mathbf{r}, \mathbf{r}') = \frac{1}{(2\pi)^3} \int e^{-i\mathbf{k} \cdot (\mathbf{r} - \mathbf{r}')} P(\mathbf{k}) d^3k + \frac{\delta^D(\mathbf{r} - \mathbf{r}')}{\bar{n}(\mathbf{r})}, \quad (65)$$

$$\mathbf{C}_{,i}(\mathbf{r}, \mathbf{r}') = \frac{\partial \mathbf{C}(\mathbf{r}, \mathbf{r}')}{\partial P(\mathbf{k}_i)} = \frac{1}{(2\pi)^3} e^{-i\mathbf{k}_i \cdot (\mathbf{r} - \mathbf{r}')}, \quad (66)$$

since  $P(\mathbf{k}) = \int P(\mathbf{k}_i) \delta^D(\mathbf{k} - \mathbf{k}_i) d^3\mathbf{k}_i$  implies that  $\partial P(\mathbf{k}) / \partial P(\mathbf{k}_i) = \delta^D(\mathbf{k} - \mathbf{k}_i)$ . As we saw in Section 4.3.1, the small-scale limit corresponds to neglecting the  $k$ -dependence of  $P$ , which gives  $\mathbf{C}(\mathbf{r}, \mathbf{r}') \approx [P + 1/\bar{n}(\mathbf{r})] \delta^D(\mathbf{r} - \mathbf{r}')$  and

$$\mathbf{C}^{-1}(\mathbf{r}, \mathbf{r}') = \left[ P + \frac{1}{\bar{n}(\mathbf{r})} \right]^{-1} \delta^D(\mathbf{r} - \mathbf{r}') = \phi(\mathbf{r}) \delta^D(\mathbf{r} - \mathbf{r}'), \quad (67)$$

where  $\phi$  is the FKP weighting function of equation (24) normalized so that  $\phi = \bar{n}/(1 + \bar{n}P)$ .

We will now rederive the FKP results with much less effort than in the previous section, by simply using the quadratic method formulas. Substituting equations (66) and (67) into equation (42) shows that the quadratic estimators  $\mathbf{q}$  are given by

$$q_i \equiv \frac{1}{2} |\hat{z}(\mathbf{k}_i)|^2, \quad (68)$$

where the function  $z(\mathbf{r}) \equiv \phi(\mathbf{r})x(\mathbf{r})/(2\pi)^3$ , which apart from a factor of  $2(2\pi)^3$  are exactly the FKP estimators of  $P(\mathbf{k})$ . Calculating the Fisher matrix by substituting equations (66) and (67) into equation (47) gives

$$\begin{aligned} \mathbf{F}_{ij} &= \frac{1}{2} \text{tr} [\mathbf{C}^{-1} \mathbf{C}_{,i} \mathbf{C}^{-1} \mathbf{C}_{,j}] \\ &\approx \frac{1}{2(2\pi)^6} \int \phi(\mathbf{r}) e^{-i\mathbf{k}_i \cdot (\mathbf{r} - \mathbf{r}')} \phi(\mathbf{r}') e^{-i\mathbf{k}_j \cdot (\mathbf{r}' - \mathbf{r})} d^3r d^3r' \\ &= \frac{1}{2(2\pi)^6} |\hat{\phi}(\mathbf{k}_i - \mathbf{k}_j)|^2. \end{aligned} \quad (69)$$

Equation (48) now gives

$$\langle q_i \rangle = \int \mathbf{F}_{ij} P(\mathbf{k}_j) d^3k_j, \quad (70)$$

which shows that the Fisher matrix is simply the 3D window function. To make the window function of the power estimate  $q_i$  integrate to unity, we need to divide it by the quantity

$$\int \mathbf{F}_{ij} d^3k_j = \frac{(2\pi)^3}{2P^2} V^{eff}, \quad (71)$$

where we have used equation (69), Parseval's theorem and equation (69) in the last step. Using equation (49), this shows that

$$\frac{\Delta q_i}{\langle q_i \rangle} \approx \sqrt{2} \frac{\int \phi(\mathbf{r}) d^3r}{\int \phi(\mathbf{r})^2 d^3r} = \sqrt{2} \left[ 1 + \frac{1}{\bar{n}P} \right], \quad (72)$$

where the last equal sign only holds for the volume limited case where  $\bar{n}$  is constant. Alternatively, averaging the power estimates  $q_i$  over a shell in  $\mathbf{k}$ -space as in the previous section, equation (49) reproduces the FKP error formula of equation (61). In summary, we have shown that the FKP method becomes lossless for measuring the power on small scales, since it equals the optimal quadratic method in this limit.

## 5. SYSTEMATIC PROBLEMS — THE SELECTION FUNCTION AND EXTINCTION

We have discussed the importance of the integral constraint in Section 3.3. Here we discuss this issue in the context of pixelized methods, and generalize it to a whole host of systematic problems, including errors in our assumed selection function  $\bar{n}(\mathbf{r})$  and our assumed extinction map.

### 5.1. What is the integral constraint?

If we knew the selection function  $\bar{n}(\mathbf{r})$  *a priori*, before counting the galaxies in our survey, we would be able to measure the power on the scale of the survey. Our power spectrum estimate would essentially be the square of the ratio of the observed and expected number of galaxies in our sample. Of course, we do not know  $\bar{n}$  *a priori*, so we use the galaxies themselves to normalize the selection function. Thus the measured density fluctuation automatically vanishes on the scale of the survey, and naive application of any of the power spectrum estimation methods we have described will falsely indicate that  $P(k) \rightarrow 0$  as  $k \rightarrow 0$ , regardless of the behavior of the true power spectrum on large scales (Peacock & Nicholson 1991).

Equation (4) tells us that apart from the noise bias  $b_i$ , there is an additional term  $W_i(\mathbf{0})$  that must be subtracted off to make  $q_i$  an unbiased power spectrum estimator. Let us assume that we know the shape of the selection function but not its normalization. To reflect this, we write the true selection function as

$$\bar{n}(\mathbf{r}) = a \bar{n}_0(\mathbf{r}), \quad (73)$$

where  $\bar{n}_0$  is our guessed selection function, and  $a$  is an unknown normalization constant, and find that our noise bias corrected power estimator will have a residual bias  $(a - 1)^2 W_i(\mathbf{0})$ . Since we do not know the exact value of  $a$ , our only way to eliminate this bias is to require that  $W_i(\mathbf{0}) = 0$ , *i.e.*, by requiring the window function to vanish at  $\mathbf{k} = \mathbf{0}$ . This was first explicitly pointed out by Fisher *et al.* (1993).

### 5.2. Its relation to extinction and other systematic problems

Since requiring  $W_i(\mathbf{0}) = 0$  eliminates the integral constraint problem, the trouble is confined to the  $\mathbf{k} = \mathbf{0}$  mode. If  $W_i(\mathbf{0}) = 0$ , then the power estimate  $q_i$  is clearly completely independent of  $P(0)$ , the fluctuations in this untrustworthy mode. The essence of our approach is therefore the following:

- We have a systematic problem with a certain mode, and can immunize our results from this problem by making them independent of this untrustworthy mode.

When phrased in this way, it is clear that this approach can be applied to a variety of other systematic problems as well. For instance, incorrectly modeled extinction adds excess power in the form of purely angular modes (density

fluctuations that have no radial component, *i.e.*, being perpendicular to the line of sight). It might therefore be desirable to make the results independent of all purely angular modes on the relevant scales or, in a less ambitious approach, at least independent of those modes whose shape coincide with known dust templates. Similarly, misestimating the *shape* of the radial selection function (of  $\bar{n}_0$  in equation (73)) pollutes certain purely radial modes which one may wish to discard.

### 5.3. How to eliminate untrustworthy modes with pixelized methods

In this section, we show how the power spectrum estimate from a pixelized method can be made insensitive to the type of systematic errors described above.

Let us parametrize the true selection function  $\bar{n}$  as

$$\bar{n}(\mathbf{r}) = \sum_{j=1}^M a_j \bar{n}_j(\mathbf{r}), \quad (74)$$

where  $\bar{n}_j$  are known functions and the parameters  $a_j$ , which we group into an  $M$ -dimensional vector  $\mathbf{a}$ , are *a priori* unknown. Imagine for example a simple case where  $M = 3$ ,  $\bar{n}_1$  is our best guess for a purely radial selection function based on a Schechter luminosity function,  $\bar{n}_2$  is a (purely angular) dust template, and  $\bar{n}_3$  gives the effect of an infinitesimal error in the estimate of the characteristic luminosity  $L_*$ :  $\bar{n}_3(\mathbf{r}) = \partial \bar{n}_1(\mathbf{r}) / \partial L_*$ . Let  $\bar{n}_0$  denote some *a priori* estimate of  $\bar{n}$ . Defining the “uncorrected” pixels as

$$x'_i \equiv \int \frac{\bar{n}(\mathbf{r})}{\bar{n}_0(\mathbf{r})} \psi_i(\mathbf{r}) d^3r, \quad (75)$$

we find that

$$\langle \mathbf{x}' \rangle = \mathbf{U} \mathbf{a}, \quad (76)$$

where the  $N \times M$  matrix  $\mathbf{U}$  of untrustworthy modes is defined by

$$\mathbf{U}_{ij} \equiv \int \frac{\bar{n}_j(\mathbf{r})}{\bar{n}_0(\mathbf{r})} \psi_i(\mathbf{r}) d^3r. \quad (77)$$

This means that in general, the data set  $\langle \mathbf{x}' \rangle \neq 0$ , so the uncorrected data set does not satisfy equation (16).

We show how to solve this problem in Appendix B. In short, one replaces  $\mathbf{x}$  by a cleaned data set  $\mathbf{\Pi x}$ , where  $\mathbf{\Pi}$  is a matrix that satisfies  $\mathbf{\Pi U} = \mathbf{0}$  and thus projects out the untrustworthy modes. We find that the best choice is  $\mathbf{\Pi} = \mathbf{I} - \mathbf{U}(\mathbf{U}^t \mathbf{C}^{-1} \mathbf{U})^{-1} \mathbf{U}^t \mathbf{C}^{-1}$ . Although the covariance matrix of the cleaned data set is not invertible, we find that with this choice of  $\mathbf{\Pi}$ , the quadratic method remains strictly optimal if we simply use  $\mathbf{C}$  from the uncleaned data in equation (43). We also show that the integral constraint correction given by equations (30) and (31) corresponds to this optimal method in the small scale limit.

## 6. PROS AND CONS OF THE METHODS

Above we have presented all methods for galaxy power spectrum estimation that have proposed in the literature, as well as the new pixelized quadratic technique and various extensions, and showed how they are related to one another. We will now discuss their relative merits at some length. It will become clear that they are highly complementary, and we summarize the pros and cons of each

method in Table 1. We will return to this in the discussion section, where we describe how the traditional, KL and quadratic methods can be used in concert to produce a data analysis pipeline having all the properties on our wish list from Section 2.

	TRAD	LIN	QUAD
Optimal on largest scales	—	+	+
Optimal on smallest scales	+	—	—
Simple & uncorrelated errors	—/+	+/-	+
Measures $z$ -space distortions	—	+	—

**Table 1:** Pros and cons of the traditional, linear (KL) and quadratic power spectrum estimation methods.

### 6.1. Pros and cons of the direct Fourier method

Unlike the pixelized methods, the traditional Fourier method uses the exact galaxy positions and thus retains all the small-scale information about  $P(k)$ .

As discussed in Section 4.3, this method becomes lossless in the limit  $k_i L \rightarrow \infty$  when the FKP choice of  $\phi$ , equation (24), is used. In addition, choosing the shell widths  $\Delta k \gg L^{-1}$  guarantees that the errors in the band power estimates  $\hat{P}_i$  will be approximately uncorrelated. This means that on small scales, say  $k_* L \ll 10\%$ , this method satisfies the first three criteria on our wish list in Section 2.

However, these advantages no longer hold when measuring power on scales comparable to the size of the survey. VS96 review problems with the direct Fourier approach that occur unless  $k_* L \ll 1$ . They fall into the two categories described below.

#### 6.1.1. The direct Fourier method destroys information

Hamilton (1997b) has shown that a strictly optimal direct summation method can be derived *in principle*, in terms of a series expansion, but this is unfortunately extremely burdensome numerically except for scales much smaller than the survey size, away from the boundaries, where it approximates equations (24) and (25). The optimal galaxy pair weighting is not separable (in the sense of equation (12)) and thus cannot be expressed in terms of a volume weighting function  $\phi$  as above. Consequently, no direct Fourier methods are lossless except on small scales.

#### 6.1.2. The method is complicated and computationally slow for large scales

It is important to note that the Fourier transformation calculation takes only a negligible amount of time in a power spectrum analysis — the lion’s share of the work involves computing the mean corrections  $W_i(\mathbf{0})$ , the shot noise correction  $b_i$ , the normalization factor  $A_i$  and the covariance matrix of the power estimates. This becomes numerically cumbersome on the largest scales, when  $k^{-1} L \sim 1$ . This is because both smearing from the window function and the effect of the integral constraint become important and must be accurately computed in this regime. Even though the relevant integrals can be greatly accelerated with FFT’s, the calculations are not only much more complicated and obscure than the simple linear algebra of the pixelized methods, but generally substantially

slower as well. The most time-consuming step is the computation of the error bars  $\Delta P$  and the covariance between power estimates using an integral constraint corrected and appropriately generalized version of equation (59), since the integral in equation (56) must be done separately for each *pair* of grid points  $(\mathbf{k}_i, \mathbf{k}_j)$  in Fourier space (cf., Goldberg & Strauss 1997). The property of uncorrelated errors is clearly lost, making it quite difficult to compute the optimal weights for averaging the power estimates in  $\mathbf{k}$ -space into power bands in  $k$ -space (T95, VS96). In short, when comparing the direct Fourier method to the KL and quadratic methods on the largest scales, it is more complicated, uses more CPU time and produces an inferior result.

## 6.2. Pros and cons of the brute force method

The pixelized brute force method has been applied to galaxy survey analysis using expansions in spherical harmonics (Fisher *et al.* 1994; Heavens & Taylor 1995; Ballinger, Taylor, & Heavens 1996).

It is arguably the simplest of all methods, both conceptually and in implementation. Moreover, it can be shown to be lossless in the limit of large data sets, thus giving minimal error bars. An important disadvantage is that it is slow. The slowest step in evaluating the likelihood function  $f$  is to compute  $\det \mathbf{C}$ , for which the CPU time required scales as  $N^3$ , and  $f$  is evaluated at a large number of grid points in the multi-dimensional parameter space. This is why it is so useful if  $N$ , the number of pixels, can be reduced by a lossless data compression scheme before performing the likelihood analysis, throwing away noise and keeping the signal. As we described above, this is exactly what the Karhunen-Loève and quadratic methods do. In the KL scheme, the compressed data set  $\mathbf{y}$  was a linear function of  $\mathbf{x}$  (of the form  $\mathbf{y} = \mathbf{B}\mathbf{x}$  for some matrix  $\mathbf{B}$ ), and in the quadratic scheme  $\mathbf{q}$  was a quadratic function of  $\mathbf{x}$ , of the form  $q_i = \mathbf{x}^\dagger \mathbf{E}_i \mathbf{x} / 2$  for some matrices  $\mathbf{E}_i$ .

A second disadvantage is that the maximum likelihood parameter estimate  $\Theta_{ml}$  (defined in Section 3.4) is such a complicated function of  $\mathbf{x}$  that we cannot calculate its statistical properties analytically. As we saw above, both the linear and quadratic schemes allow us to write down power spectrum estimators in closed form (equations (38) and (42), respectively). This allows one to compute their probability distributions exactly, (the  $y_i$  are Gaussian and the  $q_i$  are generalized  $\chi^2$  distributions, often close to Gaussian), which makes these power estimates easy to use for parameter fitting further down the data analysis pipeline.

## 6.3. Pros and cons of the KL method

### 6.3.1. It retains the phase information

An important advantage of the KL method over the others in the table is that the KL coefficients retain the spatial information about the data (not only the Fourier amplitudes, but the corresponding phases as well). This means that information on processes which affect the radial and angular clustering patterns differently can be optimally probed with the KL method. Such effects include

1. Redshift space distortions (cf., Appendix C),

2. Galactic extinction (which affects only angular modes),
3. Evolution and misestimates of  $\bar{n}(r)$  (which affect only radial modes).

We have not discussed in any detail how one might include these effects in a KL analysis. Suffice it to say that for any physical effect that affects the covariance matrix of the pixels, one can determine KL modes which are optimized for parameters which describe this effect; cf., Section 3.5.2. The way to do this for redshift-space distortions (see Appendix C) is described in more detail in TTH. We argue below in Section 6.3.4 that the simple signal-to-noise eigenmodes are appropriate general purpose modes for a KL analysis of any parameter which affects the covariance matrix only via the power spectrum. On the other hand, the KL modes should be custom tailored (using equation (39)) for parameters not in this category, such as ones causing anisotropic clustering.

Another approach is that discussed in Section 5 and Appendix B: rather than *measuring* these systematic effects, one can project out those modes that are sensitive to them, making the resulting dataset immune from them. This can be done for any pixelized method, but is especially appropriate for the quadratic method.

### 6.3.2. Pixelization is not lossless

The “–” on row 2 of Table 1 refers to the fact that computational constraints place an upper limit on the number of pixels  $N$  used for the eigenvalue problem, since the storage required scales as  $N^2$  and the CPU time as  $N^3$ .  $N = 10^4$  is readily handled on a high-end 1997 workstation (TTH), and new methods under development (Szalay & Vogeley 1997) may well be able to increase this by an order of magnitude or more, but since the dynamic range is  $\sim N^{1/3} \propto (\text{CPU time})^{1/9}$ , some information will always be lost on the very smallest scales. Fortunately, this is not a problem in practice, since the complementary traditional methods work best precisely on the smallest scales.

### 6.3.3. The KL power peak problem

For very deep surveys such as SDSS and 2dF, which probe scales substantially beyond the expected peak in the power spectrum at  $\sim 200h^{-1}\text{Mpc}$ , the KL window functions will generally not be narrow but double-peaked, since fluctuations longward of the peak have the same signal-to-noise ratio as certain fluctuations shortward of the peak and will get mixed in the corresponding KL modes. One readily circumvents this degeneracy problem by performing a likelihood analysis on the KL modes, with the band powers being the parameters to be estimated. However, the statistical errors on the resulting band power estimates will no longer be uncorrelated, and since this is a nonlinear operation, they will also not have the simple  $\chi^2$  distribution in general. This is why Table 1 indicates “+/-” in row 4: the “+” applies when we use the direct approach on a volume smaller than  $\sim 200h^{-1}\text{Mpc}$  in size, and the “–” applies when we use the indirect approach on a deep data set such as SDSS or 2dF. As was described in Section 3.5.2, one can circumvent this power peak problem by using choosing a monotonically decreasing fiducial power spectrum such as  $P(k) \propto k^{-3}$ .

### 6.3.4. The KL multi-parameter complication

The derivation of the signal-to-noise eigenmode method in *e.g.* VS96 or TTH does *not* prove that the compressed data set retains the bulk of the information about all parameters of cosmological interest, but merely that it is lossless with respect to the overall power spectrum normalization. In fact, this is not a problem in practice. TTH describe a method where one carries out a series of KL transforms, optimizing for each parameter of interest in turn, then pools all the resulting eigenmodes and uses singular value decomposition to eliminate redundancy from the pool of modes. In addition, there is good reason to believe that the information about all cosmological parameters is nonetheless preserved even with the signal-to-noise eigenmodes alone. We now give a hand-waving argument to this effect, and describe some detailed numerical experiments that support it. TTH computed three separate sets of KL modes for the CMB data set of the COBE satellite ( $N = 4016$ ), optimized for measuring three different parameters: the power spectrum normalization  $Q$ , the slope  $n$  and the reionization parameter  $\tau$ . The  $3 \times 3$  Fisher matrix was then computed from the three compressed data sets separately for  $N' = 500$  modes retained. Each set of modes retained virtually all the information about their corresponding parameter, but the error bars on  $Q$  with the  $n$  or  $\tau$  modes were substantially larger than their Cramér-Rao minimum. That is, the  $n$ -modes and the  $\tau$ -modes lost information about  $Q$ . On the other hand, the  $Q$ -modes were found to retain virtually all the information about  $n$  and  $\tau$ . Examination of their window functions revealed why. To obtain a large lever arm for determining the slope, the  $n$ -modes were probing mainly the largest and the smallest available scales, ignoring those in the middle near the “pivot point”. The  $\tau$ -modes were ignoring the very largest scales, since these are unaffected by reionization and therefore carry no information about  $\tau$ . The  $Q$ -modes, on the other hand, were faithfully probing the power on all available scales, and therefore automatically retained all of the information about  $n$  and  $\tau$  as well, as a side effect. Thus as long as the galaxy power spectrum has no sharp features (which the signal-to-noise eigenmodes might potentially ignore) we expect the standard KL modes optimized for the normalization to be close to lossless with respect to all cosmological parameters affecting only the power spectrum.

### 6.3.5. Does KL bias the results towards our theoretical prejudice?

It has been argued that the KL method biases the results by guessing an *a priori* power spectrum when computing the pixel covariance matrix. This claim has been extensively tested numerically (Bunn 1995, TTH), and found to be completely unfounded. In general, the effect of guessing an incorrect prior model is to leave the estimates unbiased, but with slightly larger error bars than what is optimal. If desired, any dependence on the initial data can clearly be eliminated by iterating the KL procedure as described in Section 4.2, while at the same time reducing the error bars close to the minimum allowed by the Fisher matrix.

A related point, true for any statistical analysis method, is that if the choice of prior has a substantial impact on the results, one is hardly learning anything from the data

anyway.

### 6.4. Pros and cons of the quadratic method

One advantage of this method is that its simple and uncorrelated quadratic estimators have narrow window functions at all  $k$ , even beyond the peak in the power spectrum. Thus it is a useful complement to the KL method on the very largest scales, as indicated by row 4 in Table 1.

A second advantage is evident from equation (42): Since the CPU time for multiplication of a vector by a matrix scales as  $N^2$ , the time for computing  $\mathbf{z}$  scales as  $N^2$  as well if equation (43) is solved by an iterative technique such as the conjugate gradient method (Press *et al.* 1992). This is much faster than the KL method, which scales as  $N^3$ . This speed increase may allow the quadratic method to be used over a somewhat larger dynamical range than the KL method, extending down to smaller scales. The quadratic method can also be used as a faster way to obtain the same results as the brute force ML method, using the iteration scheme described in Section 4.2.

Furthermore, we saw in Section 5 and Appendix B that the quadratic method can be made immune to various sorts of systematic errors which might plague the data.

An important disadvantage is that, unlike the KL method, it does not retain any phase information. This is a drawback when estimating the underlying real-space power spectrum, since although it can measure this directly by computing the appropriate  $\mathbf{C}$  once the distortion parameter  $\beta \equiv \Omega^{0.6}/b$  is known, the KL method or another linear approach must be used first, to measure  $\beta$ . Once cannot simply immunize the data from misestimates of  $\beta$  using the formalism of Appendix B, since  $\beta$  affects virtually *all* the modes. It does, however, appear possible to generalize the quadratic method to overcome this limitation (Hamilton 1997, private communication).

## 7. DISCUSSION & CONCLUSIONS

In this section, we summarize our discussion of the pros and cons of the various methods, and conclude by describing an approach combining the strengths of all of them, illustrated in Figure D1.

We found that although the direct Fourier approach is both simple to implement and virtually lossless on scales much smaller than the smallest dimension of the sample in question, it has several drawbacks on larger scales:

1. It loses information, giving unnecessarily noisy measurements.
2. It is quite tedious to implement numerically if one uses the exact expressions we have derived for the integral constraint correction, especially for computing the covariance.

In contrast, the two pixelized methods are lossless on *large* scales, but lose small-scale information because numerical constraints on the number of pixels limit the dynamical range. Since they are simpler to implement as well, they allow a more ambitious approach incorporating complications such as redshift-space distortions, residual extinction and radial selection function errors (Section 5, Appendices B and C). The quadratic method can compute exactly the same band powers as the KL method, and do so faster (the number of operations scaling as the square rather than the

cube of the number of pixels), allowing more pixels and a larger dynamical range. The KL method, on the other hand, is the only one which retains the phase information in which clustering anisotropies (differences between the angular and radial clustering patterns) is encoded. Since redshift distortions and various systematic problems manifest themselves in this way, the KL method is therefore a powerful complement to the quadratic method, since the former can quantify and subtract these systematic effects and pass the appropriate redshift-distortion parameter  $\beta$  along to the latter, which can then measure the power spectrum directly in real space as described in Appendix C. Alternatively, the quadratic method can be immunized from such systematic effects, as described in Appendix B. The KL method is also useful for cosmographic purposes, where spatial information is everything. Finally, the KL method also has the advantage of greatly simplifying trouble spotting such as search for outliers and non-Gaussian behavior.

In conclusion, we have found that although none of the methods can be made both feasible and lossless on its own, we can obtain a feasible and virtually lossless data analysis pipeline satisfying our entire wish list by combining three of them, as outlined in Figure D1.

1. The power spectrum on scales  $k^{-1} \lesssim L/10$  is estimated directly from the raw redshift data with the traditional direct Fourier approach.
2. The raw data is binned into spatial pixels substantially smaller than  $L/10$ , so that this pixelization process retains all the information except that which was already captured by the traditional method.
3. The linear (KL) method is used to measure anisotropy parameters such as  $\Omega^{0.6}/b$  (from redshift-space distortions), a residual extinction template

and corrections to the radial selection function, as well as large-scale band powers.

4. Uncorrelated estimates of the power spectrum on scales  $k^{-1} \gtrsim L/10$  are computed with the quadratic method, extending down to even smaller scales if  $N \sim 10^4 - 10^5$  pixels are feasible. This can be done both by incorporating the systematic effects found in Step 3 with the KL method, and by using quadratic estimators which are insensitive to these systematic effects. The comparison of the results for the band powers allows us to quantify how successful we are in eliminating these effects.
5. The entire process may be iterated, using the (smoothed) measured power spectrum as the fiducial one.
6. Remaining cosmological parameters are estimated with a likelihood or  $\chi^2$  analysis from the power spectrum.

This approach should allow future redshift surveys to realize their full potential to constrain cosmological models. In the meantime, it appears worthwhile to reanalyze various existing surveys with the same pipeline, to eliminate any method-induced artifacts and allow more accurate cross-comparisons of results.

We thank the Aspen Center for Physics where this paper neared its final form, and David Weinberg and Josh Frieman for useful conversations. Support for this work was provided by NASA through Hubble Fellowships HF-01078.01-94A and HF-01084.01-96A, awarded by the Space Telescope Science Institute, which is operated by AURA, Inc. under NASA contract NAS5-26555. M.A.S. acknowledges the support of the Alfred P. Sloan Foundation and NSF Grant AST96-16901.

## REFERENCES

- Baugh, C. M. & Efstathiou, G. 1994, MNRAS, 267, 323  
 Ballinger, Heavens, A., & Taylor, A. 1996, MNRAS, 276, L59  
 Bond, J. R. 1995, Phys. Rev. Lett., 74, 4369  
 Bond, J. R., Efstathiou, G. & Tegmark, M. 1997, preprint astro-ph/9702100  
 Bunn, E. F. 1995, Ph.D. Thesis, U.C. Berkeley, <ftp://pac2.berkeley.edu/pub/bunn>  
 Cole, S., Fisher, K. B. & Weinberg, D. H. (1994), MNRAS, 267, 785  
 Efstathiou, G. P. 1994, in "Les Houches Lectures 1993", eds. R. Schaeffer & J. Silk (Elsevier, Netherlands)  
 Feldman, H. A., Kaiser, N. & Peacock, J. A. 1994, ApJ, 426, 23 (FKP)  
 Fisher, K. B., Davis, M., Strauss, M. A., Yahil, A., & Huchra, J. P. 1993, ApJ, 402, 42  
 Fisher, K. B., Scharf, C. A. & Lahav, O. 1994, MNRAS, 266, 219  
 Fisher, R. A. 1935, J. Roy. Stat. Soc., 98, 39  
 Fry, J. N. 1984, ApJ, 277, L5  
 Goldberg, D. M. & Strauss, M. A. 1997, preprint astro-ph/9707209  
 Gunn, J. E., & Weinberg, D. H. 1995, in *Wide-Field Spectroscopy and the Distant Universe*, eds. S. J. Maddox and A. Aragón-Salamanca (Singapore: World Scientific), 3  
 Hamilton, A. J. S. 1992, ApJ, 385, L5  
 Hamilton, A. J. S. 1997a, preprint astro-ph/9701008, MNRAS, in press  
 Hamilton, A. J. S. 1997b, preprint astro-ph/9701009, MNRAS, in press  
 Hamilton, A. J. S. & Culhane, M. 1996, MNRAS, 278, 73  
 Heavens, A. F. & Taylor, A. N., 1995, MNRAS, 483, 497  
 Jaffe, A. H., Knox, L. & Bond, J. R. 1997, preprint astro-ph/9702109  
 Jungman, G., Kamionkowski, M., Kosowsky, A. & Spergel, D. N. 1996, Phys. Rev. D, 54, 1332  
 Kaiser, N. 1987, MNRAS, 227, 1  
 Karhunen, K., *Über lineare Methoden in der Wahrscheinlichkeitsrechnung* (Kirjapaino oy. sana, Helsinki, 1947)  
 Kendall M. G. & Stuart, A. 1969, *The Advanced Theory of Statistics*, Vol. II (Griffin, London)  
 Kenney, J. F. & Keeping, E. S. 1951, *Mathematics of Statistics, Part II*, 2nd ed. (Van Nostrand, New York)  
 Knox, L., Bond, J. R. & Jaffe, A. H. 1997, preprint astro-ph/9702110  
 Knox, L. 1997, in preparation  
 Park, C., Vogeley, M. S., Geller, M. J. & Huchra, J. P. 1994, ApJ, 431, 569  
 Peacock, J. A. 1997, MNRAS, 284, 885  
 Peacock, J. A. & Dodds, S. J. 1994, MNRAS, 267, 1020  
 Peacock, J. A. & Nicholson, D. 1991, MNRAS, 253, 307  
 Peebles, P. J. E. 1980, *The Large-Scale Structure of the Universe* (Princeton U. P., Princeton)  
 Press, W. H., Flannery, B. P., Teukolsky, S. A. & Vetterling, W. T. 1992, *Numerical Recipes* (Cambridge Univ. Press)  
 Strauss, M. A. 1997, preprint astro-ph/9610033, to appear in *Structure Formation in the Universe*, eds. A. Dekel & J. P. Ostriker  
 Strauss, M. A. & Willick, J. A. 1995, Phys. Rep., 261, 271  
 Szalay, A. & Vogeley, M. S. 1997, in preparation  
 Tegmark, M. 1995, ApJ, 455, 429 (T95)  
 Tegmark, M. 1997a, Phys. Rev. D, 55, 5895 (T97)  
 Tegmark, M. 1997b, preprint astro-ph/9706198  
 Tegmark, M. 1997c, in *Ringberg Workshop on Large-Scale Structure*, ed. D. Hamilton (Kluwer, Amsterdam)

- Tegmark, M. & Bromley, B. C. 1995, ApJ, 453, 533  
 Tegmark, M. & Hamilton, A. J. S., preprint astro-ph/9702019 (1997)  
 Tegmark, M., Taylor, A. & Heavens, A. F. 1997, ApJ, 480, 22 (TTH)  
 Vogeley, M. S. 1995, in *Wide-Field Spectroscopy and the Distant Universe*, eds. S.J. Maddox & A. Aragón-Salamanca (World Scientific, Singapore)  
 Vogeley, M. S. 1997, in *Ringberg Workshop on Large-Scale Structure*, ed. D. Hamilton (Kluwer, Amsterdam)  
 Vogeley, M. S., Park, C., Geller, M. J. & Huchra, J. P. 1992, ApJ, 391, L5  
 Vogeley, M. S. & Szalay, A. S. 1996, ApJ, 465, 34 (VS96)  
 White, M., Viana, T. P., Liddle, A. R. & Scott, D. 1996, MNRAS, 283, 107  
 Zaldarriaga, M., Seljak, U. & Spergel, D. N. 1997, preprint astro-ph/9702157  
 Zaroubi, S. & Hoffman, Y. 1996, ApJ, 462, 25

## APPENDIX



## APPENDIX A: SHOT NOISE REMOVAL

There are two basic approaches to removing shot noise in the literature. In this Appendix, we show that the two give essentially identical results.

*Using the Gaussian approximation*

Let us define write our shot noise corrected band power estimator as  $(q_i - \tilde{b}_i)$ , where  $\tilde{b}_i$  denotes our *bias correction*. Equation (4) shows that this estimator will only be unbiased if  $\langle \tilde{b}_i \rangle = b_i$ , where  $b_i$  is given by equation (8). A convenient way of removing the noise bias in pixelized methods is to choose simply  $\tilde{b} = b_i$ , since it can be done after pixelizing, without ever going back to the individual galaxy positions; for a general quadratic combination of pixels  $q_i$  as in equation (45), using equation (17) shows that the shot noise bias can be written in terms of pixelized quantities alone, as

$$b_i = \text{tr} [\mathbf{E}_i \mathbf{N}], \quad (\text{A1})$$

where  $\mathbf{N}$  is given by equation (18).

*The strict minimum variance method*

In the approximation that the shot noise fluctuations in the pixels has a Gaussian probability distribution, the above-mentioned method of choosing  $\tilde{b}_i = b_i$  is readily shown to give the unbiased power estimator with the smallest variance. This is an excellent approximation when the number of galaxies is large, as we now show. The strict minimum-variance method is (Peebles 1980) to simply omit self-pairs in equation (3):

$$q_i - \tilde{b}_i = \sum_{\alpha \neq \beta} \frac{E_i(\mathbf{r}_\alpha, \mathbf{r}_\beta)}{\bar{n}(\mathbf{r}_\alpha) \bar{n}(\mathbf{r}_\beta)}. \quad (\text{A2})$$

This corresponds to the shot noise correction

$$\tilde{b}_i = \int E_i(\mathbf{r}, \mathbf{r}) \frac{n(\mathbf{r})}{\bar{n}(\mathbf{r})^2} d^3 r = \sum_{\alpha} \frac{E_i(\mathbf{r}_\alpha, \mathbf{r}_\alpha)}{\bar{n}(\mathbf{r}_\alpha)^2}, \quad (\text{A3})$$

which is to be compared with equation (8). This is an unbiased method since  $\langle \tilde{b}_i \rangle = b_i$ . How much smaller is the variance with this approach? We illustrate this with the toy problem of estimating the power at  $k = 0$  in a volume-limited survey with  $N$  galaxies, which is simply proportional to

$$q \equiv (N - \bar{N})^2 - \tilde{b}, \quad (\text{A4})$$

where  $N$  is a Poisson-distributed random variable with mean  $\bar{N}$ . Since  $\langle (N - \bar{N})^2 \rangle = \bar{N}$ , the shot noise correction  $\tilde{b}_i = b_i$  corresponds to the choice  $\tilde{b} = \bar{N}$ . The strict minimum variance method of equation (A3) corresponds to  $\tilde{b} = N$ . Both methods are unbiased, giving  $\langle q \rangle = 0$ . The higher order moments differ, however. The variances  $\langle q^2 \rangle$  are  $2\bar{N}^2$  and  $2\bar{N}^2 + \bar{N}$ , respectively, so whereas the strictly optimal method gives the same variance that Gaussian noise would, the variance of the other method is a factor  $(1 + 1/2\bar{N})$  larger.<sup>8</sup>

<sup>8</sup> The differences between the two methods get larger for higher moments, but always remain of the order  $1/\bar{N}$ . Compared with

*Which method is preferable?*

This means that the optimal method only reduces the standard deviation by a negligible 0.01% for  $N = 10^4$  galaxies. Moreover, it is incorrect to claim that the strictly optimal method in some sense removes the “exact” shot noise: since the higher order moments depart from the Gaussian values even for this method, there is clearly Poissonian noise left in  $q$ . The difference in variance between the two methods remain equally negligible for more realistic examples, generally being of order the inverse of the number of galaxies in the survey. The choice of which method to use should therefore be dictated by practical convenience. Whereas the strict minimum variance method is of course trivial to implement in techniques involving an explicit sum over galaxy pairs (such as the FKP method), the other method is generally simpler to use for pixelized techniques, since it can be implemented using the pixelized data alone.<sup>9</sup>

## APPENDIX B: DERIVATION OF INTEGRAL CONSTRAINT AND RELATED EXPRESSIONS

In this appendix, we derive some of the results described in the text: the integral constraint correction for the traditional Fourier method (Section 3.3), and the optimal way to immunize the data from the untrustworthy modes of Section 5.

*The Integral Constraint in the Direct Fourier Method*

How should one deal with the integral constraint when using a traditional method as in Section 3.3? From the discussion in Section 5, it is clear that we should modify the weighting functions of equation (21) so that they become orthogonal to the mean density, *i.e.*, so that  $\int \psi_i(\mathbf{r}) d^3 r = 0$ . There are infinitely many ways of doing this, and some are clearly better than others if we want the power estimators  $q_i = |x_i|^2$  to retain as much cosmological information as possible. We here derive one such correction method which is both simple and intuitive, following Tegmark (1997c). We will adopt a more ambitious approach in the following subsection, deriving the optimal correction method for the pixelized case. At the end of this Appendix, we show that in the small-scale limit, the two methods are in fact identical.

If we use our guess  $\bar{n}_0$  (equation 73) in place of the unknown true selection function  $\bar{n}$  in equation (14), we will have  $\langle x_i \rangle = (a - 1) \hat{\psi}_i(0) \neq 0$ . When using a traditional power estimator  $q_i = |x_i|^2$ , this causes a systematic positive power bias  $(a - 1)^2 |\hat{\psi}_i(0)|^2$  that we cannot subtract off, as  $a$  is unknown. We must therefore modify  $\psi_i$  so that  $\hat{\psi}_i(0)$  vanishes. Let  $\hat{a}$  denote our estimate of  $a$ . We will choose  $\hat{a}$  so that this bias vanishes, *i.e.*, so that the integral

the Gaussian approximation  $\langle q^3 \rangle = 8\bar{N}^3$ , the skewness of the two methods is up by factors of  $(1 + 2/\bar{N})$  and  $(1 + 11/4\bar{N} + 1/8\bar{N}^2)$ , and compared with the Gaussian approximation  $\langle q^4 \rangle = 60\bar{N}^4$ , the kurtosis is up by factors of  $(1 + 12/5\bar{N} + 2/15\bar{N}^2)$  and  $(1 + 33/5\bar{N} + 23/12\bar{N}^2 + 1/60\bar{N}^3)$ .

<sup>9</sup> There is one useful exception: one can use the strict minimum variance method based on pixelized data alone in the special case where the pixels are counts in (sharp-edged) cells, in which case the terms  $x_i^2$  get replaced by  $x_i(x_i - 1)$ .

constraint

$$\int \left[ \frac{n(\mathbf{r})}{\hat{a}\bar{n}_0(\mathbf{r})} - 1 \right] \phi(\mathbf{r}) d^3r = 0 \quad (\text{B1})$$

holds, or explicitly,

$$\hat{a} \equiv \frac{1}{\hat{\phi}(\mathbf{0})} \int \frac{n(\mathbf{r})}{\bar{n}_0(\mathbf{r})} \phi(\mathbf{r}) d^3r. \quad (\text{B2})$$

This is an unbiased estimator of the density normalization, since  $\langle \hat{a} \rangle = a$ , the true value. Substituting  $\bar{n}(\mathbf{r}) = \hat{a}\bar{n}_0(\mathbf{r})$  and equations (21) and (B2) into equation (14), we obtain

$$\begin{aligned} x_i &= \frac{1}{\hat{a}} \left[ \int \frac{n(\mathbf{r})}{\bar{n}_0(\mathbf{r})} e^{i\mathbf{k}_i \cdot \mathbf{r}} \phi(\mathbf{r}) d^3r - \hat{\phi}(\mathbf{k}_i) \hat{a} \right] \\ &= \frac{1}{\hat{a}} \left[ \int \frac{n(\mathbf{r})}{\bar{n}_0(\mathbf{r})} e^{i\mathbf{k}_i \cdot \mathbf{r}} \phi(\mathbf{r}) d^3r - \frac{\hat{\phi}(\mathbf{k}_i)}{\hat{\phi}(\mathbf{0})} \int \frac{n(\mathbf{r})}{\bar{n}_0(\mathbf{r})} \phi(\mathbf{r}) d^3r \right] \\ &= \frac{a}{\hat{a}} \int \frac{n(\mathbf{r})}{\bar{n}(\mathbf{r})} \psi_i(\mathbf{r}) d^3r \approx \int \frac{n(\mathbf{r})}{\bar{n}(\mathbf{r})} \psi_i(\mathbf{r}) d^3r, \end{aligned} \quad (\text{B3})$$

where the function  $\psi_i$  is defined by

$$\psi_i(\mathbf{r}) \equiv \left[ e^{i\mathbf{k}_i \cdot \mathbf{r}} - \frac{\hat{\phi}(\mathbf{k}_i)}{\hat{\phi}(\mathbf{0})} \right] \phi(\mathbf{r}). \quad (\text{B4})$$

Hence its Fourier transform is

$$\hat{\psi}_i(\mathbf{k}) = \hat{\phi}(\mathbf{k} - \mathbf{k}_i) - \frac{\hat{\phi}(\mathbf{k}_i)}{\hat{\phi}(\mathbf{0})} \hat{\phi}(\mathbf{k}). \quad (\text{B5})$$

The relative error in  $\hat{a}$  is of order the inverse square root of the number of galaxies in the survey, so we can to a good approximation treat  $a$  as a known constant from here on and take  $a/\hat{a} = 1$  on the last line of equation (B3). We see that the volume weighting  $\psi_i$  given by equation (B4) is better than the traditional choice of equation (21) since it is orthogonal to the mean, *i.e.*, it satisfies  $\hat{\psi}_i(\mathbf{0}) = 0$ , which guarantees that  $\langle x_i \rangle = 0$ .

In practice, we need never use equation (B4) to compute  $x_i$  with equation (14), since this is implicitly done if we first correct  $\bar{n}$  by estimating its normalization with equation (B2) and then apply the simple weight function of equation (21). (This is mathematically equivalent to applying the weight function equation (B4) directly to the data, using an arbitrary  $\bar{n}$ -normalization.) However, we do need equation (B4) to derive the expressions for the shot noise correction and normalization given in Equations (31) and (30). Substituting equation (B4) into equation (8) gives the shot noise correction

$$\begin{aligned} b_i &= \int \frac{|\psi_i(\mathbf{r})|^2}{\bar{n}(\mathbf{r})} d^3r \\ &= \int \left| e^{i\mathbf{k}_i \cdot \mathbf{r}} - \frac{\hat{\phi}(\mathbf{k}_i)}{\hat{\phi}(\mathbf{0})} \right|^2 \frac{\phi(\mathbf{r})^2}{\bar{n}(\mathbf{r})} d^3r, \end{aligned} \quad (\text{B6})$$

and expanding the square completes our derivation of equation (31). The normalization coefficient  $A_i$  of equation (29) is determined by the requirement that the window function integrate to unity, *i.e.*,  $A_i = \int |\hat{\psi}_i(\mathbf{k})|^2 d^3k / (2\pi)^3$ .

Using Parseval's theorem, we obtain

$$\begin{aligned} A_i &= \int |\psi_i(\mathbf{r})|^2 d^3r \\ &= \int \left| e^{i\mathbf{k}_i \cdot \mathbf{r}} - \frac{\hat{\phi}(\mathbf{k}_i)}{\hat{\phi}(\mathbf{0})} \right|^2 \phi(\mathbf{r})^2 d^3r, \end{aligned} \quad (\text{B7})$$

and expanding the square as above completes our derivation of equation (30).

*How important is this correction?*

Let us evaluate the integral constraint correction factor  $A_i$  for a couple of simple examples. We first note that for the special case of equation (22), we have  $\phi(\mathbf{r})^2 \propto \phi(\mathbf{r})$ . Hence  $a(\mathbf{k}) \propto \hat{\phi}(\mathbf{k})$ , and equation (30) reduces to

$$A_i = \left( 1 - \left| \frac{\hat{\phi}(\mathbf{k}_i)}{\hat{\phi}(\mathbf{0})} \right|^2 \right) a(\mathbf{0}), \quad (\text{B8})$$

which we recognize as the result of Park *et al.* (1994). For volume-limited surveys, the prescriptions given by equations (22), (23) and (24) all coincide, so this expression is exact for the volume-limited case with these galaxy weighting schemes. For flux-limited surveys, on the other hand, these schemes all give a decreasing weight function  $\psi$ , since  $\bar{n}$  decreases with distance. For the simple Gaussian case  $\phi(\mathbf{r}) = \exp[-(r/R)^2/2]/\pi^{1/4}R^{1/2}$ , equation (30) gives

$$A_i = 1 + e^{-(Rk_i)^2} - 2e^{-\frac{3}{4}(Rk_i)^2}, \quad (\text{B9})$$

whereas the approximation (B8) gives

$$A_i = 1 - e^{-(Rk_i)^2}. \quad (\text{B10})$$

A Taylor expansion shows that for  $kR \ll 1$ , the latter overestimates  $A_i$  by a factor of two as illustrated in Figure 2.

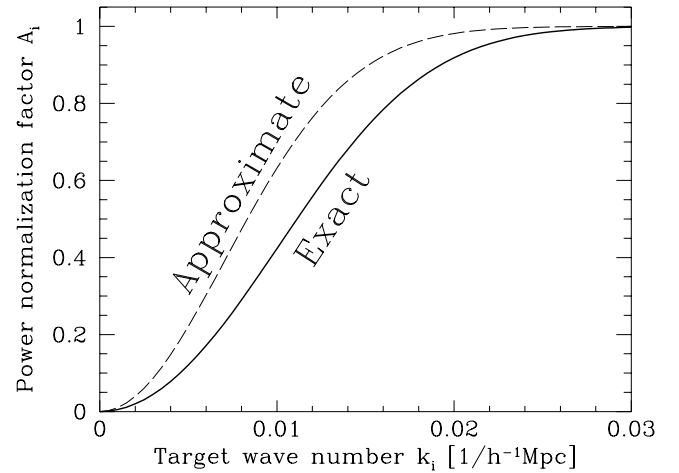


**FIG. 2** — The exact expression for the integral constraint correction  $A_i$  is plotted together with the approximation of Park *et al.* (1994) for a Gaussian weight function  $\psi(\mathbf{r}) \propto \exp[-(r/R)^2/2]$ ,  $R = 100h^{-1}\text{Mpc}$ .

*Eliminating contaminated modes with pixeled methods:  
A Simple Solution*

In this and the next subsection, we continue the discussion of Section 5, and present a method to project out modes of the density field that we believe might be contaminated by, *e.g.*, errors in the selection function or in the assumed extinction map. Our starting point is equation (77), the  $N \times M$  matrix  $\mathbf{U}$  of untrustworthy modes.

To remedy the problem, we construct a new “cleaned” data set that is independent of  $\mathbf{a}$ , the coefficients of these modes. Let us define

$$\mathbf{x} \equiv \mathbf{\Pi} \mathbf{x}', \quad (\text{B11})$$

where  $\mathbf{\Pi}$  is an  $N \times N$  matrix satisfying

$$\mathbf{\Pi} \mathbf{U} = \mathbf{0}, \quad (\text{B12})$$

*i.e.*, having the columns of  $\mathbf{U}$  in its null space. This implies that  $\mathbf{\Pi}$  has at most rank  $N - M$ . We will choose it to have exactly this rank, since otherwise  $\mathbf{\Pi}$  will destroy more information than necessary (for instance, null matrix choice  $\mathbf{\Pi} = \mathbf{0}$  satisfies equation (B12), but destroys all our information). It is easy to construct such matrices, a simple choice being

$$\mathbf{\Pi} = \mathbf{I} - \mathbf{U}(\mathbf{U}^t \mathbf{U})^{-1} \mathbf{U}^t. \quad (\text{B13})$$

This is the symmetric ( $\mathbf{\Pi}^t = \mathbf{\Pi}$ ) projection matrix ( $\mathbf{\Pi}^2 = \mathbf{\Pi}$ ) projecting onto the subspace orthogonal to the columns of  $\mathbf{U}$ . Our corrected data set  $\mathbf{x}$  satisfies equation (16), since  $\langle \mathbf{x} \rangle = \mathbf{\Pi} \mathbf{U} \mathbf{a} = \mathbf{0}$ . Letting  $\mathbf{C}'$  denote the covariance matrix of the uncorrected data set, the corrected data will have the covariance matrix

$$\mathbf{C} \equiv \langle \mathbf{x} \mathbf{x}^t \rangle = \mathbf{\Pi} \mathbf{C}' \mathbf{\Pi}^t. \quad (\text{B14})$$

Once  $\mathbf{x}$  and  $\mathbf{C}$  have been computed, the rest of the pixelized analysis proceeds just as described in Sections 3.4, 3.5 or 3.6. The only complication is that  $\mathbf{C}$  is now singular, having rank  $N - M$  instead of  $N$ . As shown in the Appendix of T97, the correct way to deal with this in the quadratic method is to replace all occurrences of  $\mathbf{C}^{-1}$  (which is of course undefined) by the “pseudo-inverse” of  $\mathbf{C}$ , defined as

$$\mathbf{\Pi} [\mathbf{C} + \gamma \mathbf{U} \mathbf{U}^t]^{-1} \mathbf{\Pi} \quad (\text{B15})$$

for some constant  $\gamma \neq 0$ . T97 shows that the result is independent of  $\gamma$ , and that a good choice for numerical stability is  $\gamma \sim c/N$ , where  $c$  is the order of magnitude of a typical matrix element of  $\mathbf{C}$ . The same trick can be used for the KL method, in the step where equation (39) is reduced to an ordinary eigenvalue problem by Cholesky decomposing  $\mathbf{C}$  as described in TTH.

*The optimal solution*

Equation (B13) does not give the only rank  $N - M$  projection matrix satisfying  $\mathbf{\Pi} \mathbf{U} = \mathbf{0}$  — there are in fact infinitely many such matrices of the form  $\mathbf{\Pi} = \mathbf{I} - \mathbf{U}(\mathbf{U}^t \mathbf{M} \mathbf{U})^{-1} \mathbf{U}^t \mathbf{M}$ , where  $\mathbf{M}$  is an arbitrary non-singular matrix, and equation (B13) simply corresponds to the case  $\mathbf{M} \propto \mathbf{I}$ . Since they all have the same null space  $\mathbf{U}$ , it is clear that they all destroy the same information (all the information about the untrustworthy modes, no more and no

less). The power spectrum Fisher matrix for the cleaned data set is therefore independent of  $\mathbf{M}$ , so our choice is purely one of numerical convenience. For the quadratic method in particular, there turns out to be a much more appropriate choice than that of equation (B13), which altogether eliminates the above-mentioned problem of  $\mathbf{C}$  being singular by allowing the quadratic pair weighting  $\mathbf{E}$  to be computed analytically. We will derive this choice of  $\mathbf{\Pi}$  by generalizing the derivation of the quadratic method (T97) to include our constraint that the results be independent of the corrupted modes.

The most general quadratic estimator can clearly be written as in equation (45) for some symmetric matrix  $\mathbf{E}_i$ . As shown in T97, this implies that the variance of  $q_i$  is given by

$$V(q_i) \equiv \langle q_i^2 \rangle - \langle q_i \rangle^2 = \frac{1}{2} \text{tr} [\mathbf{C} \mathbf{E}_i \mathbf{C} \mathbf{E}_i] \quad (\text{B16})$$

and that the signal, the expected contribution to  $q_i$  from the power band of interest, is  $\text{tr} [\mathbf{C}_{,i} \mathbf{E}_i]/2$ , where  $\mathbf{C}_{,i}$  is defined by equation (44). To maximize the signal-to-noise ratio, we want to minimize the variance given a fixed signal, *i.e.*, subject to the constraint that  $\text{tr} [\mathbf{C}_{,i} \mathbf{E}_i]$  is held constant. If we write

$$q_i = \frac{1}{2} (\mathbf{x} + \mathbf{U} \mathbf{a})^t \mathbf{E}_i (\mathbf{x} + \mathbf{U} \mathbf{a}), \quad (\text{B17})$$

it is clear that we can phrase our constraint on  $\mathbf{E}_i$  as  $\mathbf{E}_i \mathbf{U} = \mathbf{0}$ . This is in fact  $N \times M$  separate constraint equations, so using the fact that  $\mathbf{E}_i$  is symmetric, our constrained minimization problem involves minimizing

$$L \equiv \text{tr} \left\{ \frac{1}{2} \mathbf{C} \mathbf{E}_i \mathbf{C} \mathbf{E}_i - \lambda \mathbf{C}_{,i} \mathbf{E}_i + \lambda [\mathbf{U} \mathbf{A}^t + \mathbf{A} \mathbf{U}^t] \mathbf{E}_i \right\}, \quad (\text{B18})$$

where  $\mathbf{A}$  is some arbitrary  $N \times M$  matrix of Lagrange multipliers. Requiring the derivatives with respect to the components of  $\mathbf{E}_i$  to vanish, we obtain

$$\mathbf{E}_i \propto \mathbf{C}^{-1} [\mathbf{C}_{,i} - \mathbf{U} \mathbf{A}^t - \mathbf{A} \mathbf{U}^t] \mathbf{C}^{-1}, \quad (\text{B19})$$

where  $\mathbf{A}$  is determined by the constraint  $\mathbf{E}_i \mathbf{U} = \mathbf{0}$ . Defining  $\tilde{\mathbf{U}} \equiv \mathbf{C}^{-1} \mathbf{U}$ , the solution is

$$\mathbf{A} = \left[ \mathbf{I} - \frac{1}{2} \mathbf{U} (\tilde{\mathbf{U}}^t \mathbf{U})^{-1} \tilde{\mathbf{U}}^t \right] \mathbf{C}_{,i} \tilde{\mathbf{U}} (\tilde{\mathbf{U}}^t \mathbf{U})^{-1}, \quad (\text{B20})$$

which can be verified by direct substitution. Substituting this back into equation (B19) finally yields

$$\mathbf{E}_i \propto \mathbf{\Pi}^t \mathbf{C}^{-1} \mathbf{C}_{,i} \mathbf{C}^{-1} \mathbf{\Pi}, \quad (\text{B21})$$

where

$$\mathbf{\Pi} = \mathbf{I} - \mathbf{U} (\mathbf{U}^t \tilde{\mathbf{U}})^{-1} \tilde{\mathbf{U}}^t = \mathbf{I} - \mathbf{U} (\mathbf{U}^t \mathbf{C}^{-1} \mathbf{U})^{-1} \mathbf{U}^t \mathbf{C}^{-1} \quad (\text{B22})$$

is a projection matrix satisfying  $\mathbf{\Pi} \mathbf{U} = \mathbf{0}$ ,  $\mathbf{\Pi}^t \tilde{\mathbf{U}} = \mathbf{0}$  and  $\mathbf{C}^{-1} \mathbf{\Pi} = \mathbf{\Pi}^t \mathbf{C}^{-1}$ . Inserting equation (B21) into equation (45), we see that our quadratic estimator retains the simple form of equation (42) if we generalize equation (43) to

$$\mathbf{z} \equiv \mathbf{C}^{-1} \mathbf{\Pi} \mathbf{x}, \quad (\text{B23})$$

so after cleaning the data set (replacing  $\mathbf{x}$  by  $\mathbf{\Pi x}$ ), the quadratic method proceeds exactly as before. This generalization of the quadratic method clearly reduces to the prescription in Section 3.6 ( $\mathbf{z} = \mathbf{C}^{-1}\mathbf{x}$ ) if there are no untrustworthy modes, in which case  $M = 0$  and  $\mathbf{\Pi} = \mathbf{I}$ . Note that this technique is quite useful for estimating the power spectrum from cosmic microwave background experiments as well, in which case obvious candidates for corrupted modes are the monopole and the three dipole components.

#### Relation between the pixelized and continuous cleaning schemes

In this section, we will show that the integral correction procedure for traditional methods that we derived above is lossless for the FKP volume weighting in the small-scale limit, corresponding to the quadratic method.

When we have merely one untrustworthy mode ( $M = 1$ ) corresponding to the normalization of  $\bar{n}$ , the matrix defined by equation (77) consists of a single column vector;  $\mathbf{U} = \mathbf{u}$ . Using the continuum pixels  $x(\mathbf{r})$  of equation (63), this vector is simply the  $\mathbf{k} = \mathbf{0}$  (constant) mode, *i.e.*,

$$u(\mathbf{r}) = 1. \quad (\text{B24})$$

Let us now evaluate the optimal power estimate  $q_i$  that we derived above, given by Equations (42) and (B23). Since  $\mathbf{U} = \mathbf{u}$ , we have

$$\mathbf{\Pi x} = \mathbf{x} - \left( \frac{\mathbf{u}^t \mathbf{C}^{-1} \mathbf{x}}{\mathbf{u}^t \mathbf{C}^{-1} \mathbf{u}} \right) \mathbf{u}, \quad (\text{B25})$$

where Equations (67) and (B24) show that  $\mathbf{u}^t \mathbf{C}^{-1} \mathbf{x} = \int \phi(\mathbf{r}) x(\mathbf{r}) d^3 r$  and  $\mathbf{u}^t \mathbf{C}^{-1} \mathbf{u} = \int \phi(\mathbf{r}) d^3 r = \hat{\phi}(0)$ . We can thus write

$$z(\mathbf{r}) = (\mathbf{C}^{-1} \mathbf{\Pi x})(\mathbf{r}) = \int \left[ \delta^D(\mathbf{r} - \mathbf{r}') - \frac{\phi(\mathbf{r})}{\hat{\phi}(0)} \right] \phi(\mathbf{r}') x(\mathbf{r}') d^3 r'. \quad (\text{B26})$$

Fourier transforming this with respect to  $\mathbf{r}'$ , Equation (68) now shows that  $q_i = |x_i|^2/2$ , where

$$x_i = \hat{z}(\mathbf{k}_i) = \int \psi_i(\mathbf{r}) x(\mathbf{r}) d^3 r, \quad (\text{B27})$$

and the volume weighting function  $\psi_i$  is exactly the one that we derived in Section B.1, given by equation (B4). In other words, we have shown that the FKP choice of the function  $\phi$  together with the volume weighting of equation (B4) is identical to the lossless quadratic method in the small-scale limit.

## APPENDIX C: REDSHIFT DISTORTIONS AND CLUSTERING EVOLUTION

In Section 5 and Appendix B, we showed that the pixelized methods allow a more ambitious approach than is feasible with the direct Fourier methods, incorporating multiple integral constraints, since all the complications simply became buried in the appropriate matrices. In this Appendix, we show how two additional complications can be incorporated with pixelized methods in the same vein: redshift distortions and clustering evolution.

### Redshift distortions

A ubiquitous problem with power spectrum estimation is that of “redshift distortions”. When estimating the distance to a galaxy by its redshift, galaxies receding faster than the Hubble flow due to local gravitational interactions appear to be further away than they really are, and vice versa. This was first discussed by Kaiser (1987) in the context of  $P(k)$ , and a recent review is given by Tegmark & Bromley (1995). Denoting the apparent density field in redshift space  $\delta_s(\mathbf{r})$ , it is straightforward to use Kaiser’s formalism to show that for a volume limited survey in linear perturbation theory (Hamilton & Culhane 1996),

$$\delta_s = \left[ 1 + \beta \left( \frac{\partial^2}{\partial r^2} + \frac{\alpha(\mathbf{r})}{r} \frac{\partial}{\partial r} \right) \nabla^{-2} \right] \delta_r, \quad (\text{C1})$$

where  $\beta \equiv \Omega^{0.6}/b$ , the constant  $b$  is the so called bias factor, and

$$\alpha(\mathbf{r}) \equiv 2 + \frac{\partial \ln \bar{n}(\mathbf{r})}{\partial \ln r} \quad (\text{C2})$$

is the logarithmic slope of the radial selection function (plus two). Fourier transforming this gives (Hamilton & Culhane 1996)

$$\hat{\delta}_s(\mathbf{k}) = \hat{\delta}_r(\mathbf{k}) + \beta \int f(\mathbf{k}, \mathbf{k}') \hat{\delta}_r(\mathbf{k}') d^3 k', \quad (\text{C3})$$

where the function  $f$  is defined by

$$f(\mathbf{k}, \mathbf{k}') \equiv \int e^{i(\mathbf{k}' - \mathbf{k}) \cdot \mathbf{r}} \left[ (\hat{\mathbf{k}}' \cdot \hat{\mathbf{r}})^2 - \frac{\alpha(\mathbf{r})}{k'r} (\hat{\mathbf{k}}' \cdot \hat{\mathbf{r}}) \right] d^3 r. \quad (\text{C4})$$

Thus we obtain

$$\langle \hat{\delta}_s(\mathbf{k}) \hat{\delta}_s(\mathbf{k}') \rangle = (2\pi)^3 \int g(\mathbf{k}, \mathbf{k}', \mathbf{k}'') P(\mathbf{k}'') d^3 k'', \quad (\text{C5})$$

where

$$\begin{aligned} g(\mathbf{k}, \mathbf{k}', \mathbf{k}'') &\equiv \delta^D(\mathbf{k} - \mathbf{k}'') \delta^D(\mathbf{k}' - \mathbf{k}'') + \\ &+ \beta [\delta^D(\mathbf{k} - \mathbf{k}'') f(\mathbf{k}', \mathbf{k}) + \delta^D(\mathbf{k}' - \mathbf{k}'') f(\mathbf{k}, \mathbf{k}')^*] + \\ &+ \beta^2 f(\mathbf{k}, \mathbf{k}'')^* f(\mathbf{k}', \mathbf{k}''). \end{aligned} \quad (\text{C6})$$

The above expressions are derived and discussed in detail by Zaroubi & Hoffman (1996), and also in Tegmark & Bromley (1995) and T95 for the volume limited case. The key point here is that although  $\langle \hat{\delta}_s(\mathbf{k}) \hat{\delta}_s(\mathbf{k}') \rangle$  is no longer diagonal, and rather messy, it is still linear in the power spectrum. Thus the pixel covariance matrix  $\mathbf{C}$  will still be some shot noise term plus a term *linear* in  $P(\mathbf{k})$ . In other words, by letting  $\mathbf{C}_{,i}$  refer to the derivative of  $\mathbf{C}$  with respect to the band powers in *real* space instead of redshift space, the quadratic method will measure the real space power spectrum directly (given *a priori* knowledge of  $\beta$ ), and the corresponding window functions (the rows of  $\mathbf{F}$ , say) will show the contributions to the measurements  $q_i$  from the various real space power bands.

### Clustering evolution

The density fluctuation field  $\delta_r$  maintains its shape in linear perturbation theory, simply increasing in amplitude by a position-independent growth factor  $D$ . Since we are

seeing distant galaxies at an earlier time, we see the apparent density fluctuations

$$\delta_a(\mathbf{r}) \equiv D(r)\delta_r(\mathbf{r}), \quad (\text{C7})$$

where  $D(r) = 1/(1+z)$  for  $\Omega = 1$ . This effect is straightforward to include in a pixelized analysis. Equation (18) remains unchanged and equation (19) simply gets replaced by

$$\mathbf{S}_{ij} = \frac{1}{(2\pi)^3} \int \hat{\psi}'_i(\mathbf{k}) \hat{\psi}'_j(\mathbf{k})^* P(k) d^3k, \quad (\text{C8})$$

where we have defined the functions  $\psi'_i(\mathbf{r}) \equiv D(r)\psi_i(\mathbf{r})$ . This correction is quite small for shallow galaxy surveys, where  $\bar{n}$  typically varies dramatically between  $z = 0$  and  $z = 0.2$ , a range over which  $D$  changes by at most about 20%, less for small  $\Omega$ . If this effect is incorporated into the analysis,  $\Omega$  can be made a free parameter to be fit for in the pipeline.

This clustering evolution should not be confused with galaxy evolution, which we do not discuss here, and which affects only  $\bar{n}$ , not  $\delta_r$ .

#### APPENDIX D: NORMALIZATION CONVENTIONS

Unfortunately, the power spectrum  $P(k)$  is defined in many different ways in the literature, differing by normalization factors such as  $(2\pi)^3$  and a fiducial box volume  $V$ . In this paper, we normalize Fourier transforms as

$$\hat{f}(\mathbf{k}) \equiv \int f(\mathbf{r}) e^{-i\mathbf{k}\cdot\mathbf{r}} d^3r, \quad (\text{D1})$$

and normalize  $P(k)$  so that

$$\langle \hat{\delta}_r(\mathbf{k})^* \hat{\delta}_r(\mathbf{k}') \rangle = (2\pi)^3 \delta^D(\mathbf{k} - \mathbf{k}') P(k). \quad (\text{D2})$$

The units of  $P(k)$  are volume. With this normalization, the dimensionless power  $\Delta^2$  of Peacock & Dodds (1994) is given by

$$\Delta^2(k) = \frac{4\pi}{(2\pi)^3} k^3 P(k), \quad (\text{D3})$$

the r.m.s. fluctuations  $\sigma_8$  in a sphere of radius  $R = 8h^{-1}$  Mpc are

$$\sigma_8^2 = \frac{1}{2\pi^2} \int_0^\infty \left[ \frac{\sin x - x \cos x}{x^3/3} \right]^2 P(k) k^2 dk, \quad (\text{D4})$$

where  $x \equiv kR$ , and the Sachs-Wolfe quadrupole  $Q$  in the cosmic microwave background is given by

$$Q^2 \equiv \frac{5}{4\pi} C_2 = \frac{10}{\pi^2} \int_0^\infty \frac{j_2(x)^2}{x^4} P(k) k^2 dk, \quad (\text{D5})$$

where  $x \approx 2kc/H_0 \approx k \times 6000h^{-1}$  Mpc and

$$j_2(x) = \frac{3 \sin x - 3x \cos x - x^2 \sin x}{x^3}. \quad (\text{D6})$$

T95 uses a convention where the  $(2\pi)^3$  factor in equation (D2) is replaced by  $(2\pi)^6$ .

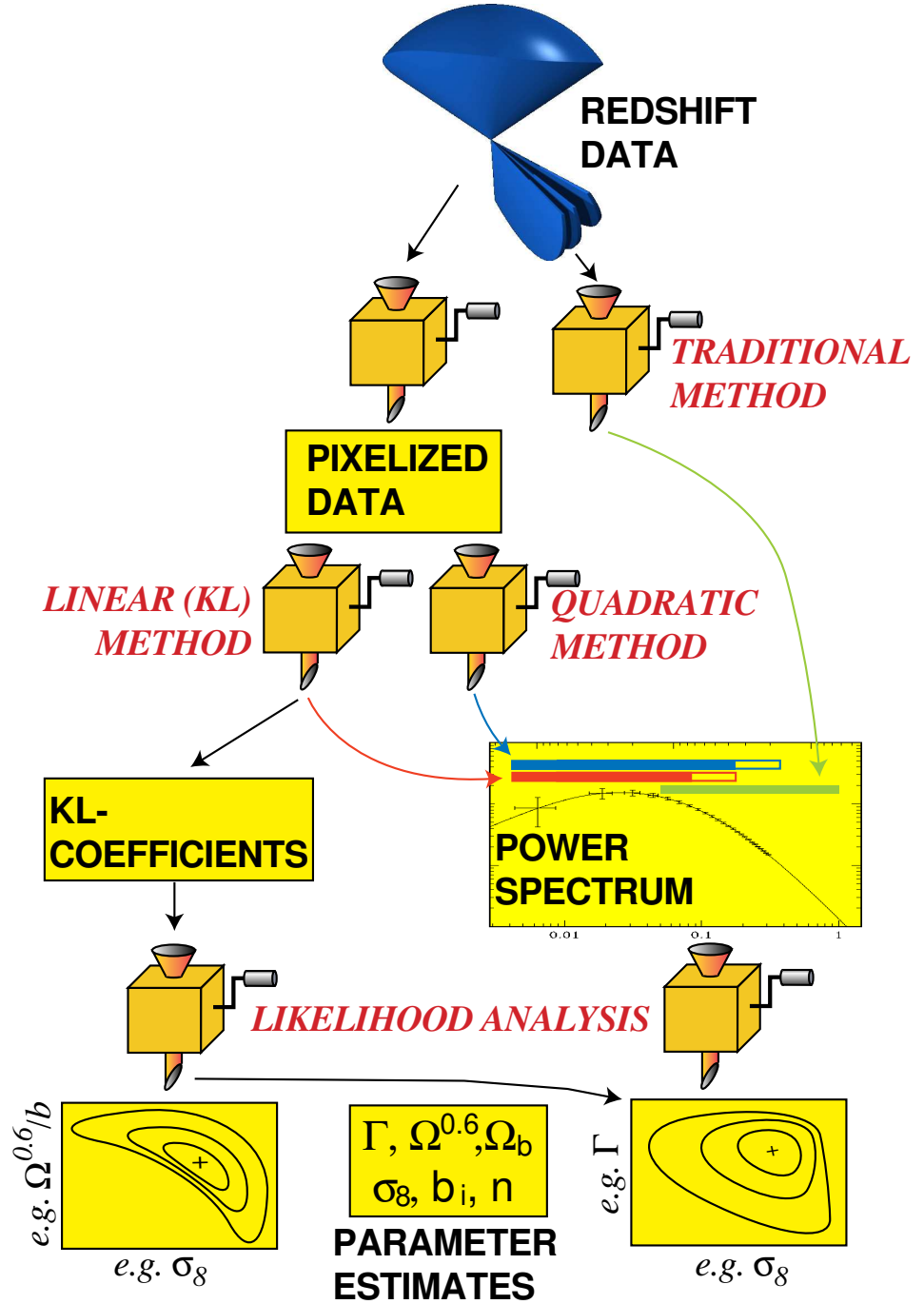


FIG. D1.— We propose analyzing large future galaxy redshift surveys such as the SDSS by using three techniques in conjunction: a traditional Fourier approach on small scales, a pixelized quadratic matrix method on large scales and a pixelized Karhunen-Loève eigenmode analysis to probe anisotropic effects such as redshift-space distortions and residual extinction. The horizontal bars in the power spectrum box indicate that the quadratic method has a larger dynamic range than the KL method. The bottom of the figure indicates that numbers such as the redshift distortion parameter  $\Omega^{0.6}/b$  which reflect anisotropic clustering can only be optimally constrained using the KL modes, which retain not merely the overall power, but the phase information as well.